A state parameter-based thermomechanical constitutive model for saturated fine-grained soils

Dr. **Qi-Yin ZHU**, associate professor

Email: qiyin.zhu@cumt.edu.cn

State Key Laboratory for Geomechanics and Deep Underground Engineering, China University of Mining & Technology, Xuzhou 221116, China

Dr. **Pei-Zhi ZHUANG**

Corresponding author

Email: p.zhuang@leeds.ac.uk

School of Qilu Transportation, Shandong University, 250002, Jinan, China

Formerly at School of Civil Engineering, University of Leeds, LS2 9JT Leeds, UK

Dr. **Zhen-Yu YIN**, associate professor

Email: zhenyu.yin@polyu.edu.hk

Department of Civil and Environmental Engineering, Hong Kong Polytechnic University, Hung Hom, Kowloon, Hong Kong, China

Professor **Hai-Sui YU,** FREng

Deputy Vice-Chancellor

E-mail: H.Yu@leeds.ac.uk

School of Civil Engineering, University of Leeds, LS2 9JT Leeds, UK

Approx. 6600 words 1 Table, 15 Figures

Revised manuscript on 22 January 2020

ABSTRACT

This paper presents a two-surface constitutive model for describing thermomechanical behaviour of saturated fine-grained soils at both normally consolidated and overconsolidated states. A thermal dependent stress ratio-state parameter relation is adopted to account for the effects of temperature on the shape of the state boundary surface (SBS) of soils. In the model, both the size and the shape of the SBS are allowed to vary with temperature, which is evidenced by thermal variation of the mechanical yield loci and the shifts of the normal consolidation line (NCL) and the critical state line (CSL) upon heating and/or cooling. A thermal yield surface is added for modelling the isotropic thermal deformation of soils more accurately, in particular at overconsolidated states. The mechanical and thermal yield mechanisms are coupled by the temperature dependent preconsolidation pressure which is controlled by a volumetric hardening law. Based on experimental observations, a nonlinear relationship between the spacing ratio and temperature changes is defined and a thermal dependent non-associated flow rule is proposed. The model is validated against some selected experimental results of several soils tested under various mechanical and thermal paths such as drained isotropic heating and cooling, drained and undrained triaxial compression at non-isothermal conditions.

KEYWORDS: Temperature effects, Constitutive relations, Clays, Plasticity, State parameter

Introduction

Significant temperature changes in soils may occur due to daily and seasonal temperature variations, heat transfer between geothermal structures and the surrounding soil (Bourne-Webb et al. 2016; Laloui and Di Donna 2013), heat release of nuclear waste disposal (Baldi et al. 1991; Graham et al. 1997) and energy dissipation during soil deformation (Pinyol et al. 2017). The thermomechanical behaviour of soils may greatly affect the stability of soil itself and the safety and performance of associated geostructures (e.g., pavement (Teltayev and Suppes 2019), energy piles, tunnels and walls (Barla et al. 2016; Bourne-Webb et al. 2019; Di Donna et al. 2017; Laloui et al. 2006), buried pipes and cables (di Schio et al. 2016; Mitchell and Abdel-hadi 1979), petroleum drilling (Chen et al. 2003; Li et al. 2019)). Thus, understanding and modelling of the effects of temperature changes on the engineering properties of soils have been the subject of many studies in environmental geomechanics.

After the pioneering work by Campanella and Mitchell (1968), extensive experimental investigations on the thermomechanical behaviour of soils, particularly water-saturated clays, have been conducted (for example, (Abuel-Naga et al. 2007b; Baldi et al. 1991; Cekerevac and Laloui 2004; Ghahremannejad 2003; Hueckel and Baldi 1990; Kuntiwattanakul et al. 1995; Ng et al. 2018; Shetty et al. 2019; Sultan et al. 2002; Tanaka et al. 1997; Towhata et al. 1993; Uchaipichat and Khalili 2009)). It was shown that temperature strongly affects the behaviour of fine-grained soils mainly through its influences on the soil structure and the free and absorbed water. Thorough discussions on the main thermomechanical behaviour of saturated clays from the perspective of constitutive modelling were made by Cui et al. (2000), Laloui and François (2009) and Mašín and Khalili (2012), among others. Here some important and general characteristics are summarised as follows:

(a) Temperature influences the NCL of a soil; NCLs at different temperatures are approximately parallel to each other in the semi-logarithmic v-ln$p$ plot (p: mean effective stress; v: soil specific volume);

(b) Heating a saturated soil under drained conditions induces volume changes that strongly depends on the stress history (e.g., the overconsolidation ratio (OCR));

(c) The size and the shape of the yield surface are temperature dependent; thermal loadings could lead to either an increase or a decrease in the soil peak strength.

Based on experimental observations, various thermomechanical constitutive models were proposed over the past three decades taking some well-validated isothermal mechanical soil models as the basis. The basic framework for modern thermoplasticity constitutive modelling is largely attributed to the pioneering work by Hueckel and Borsetto (1990) and Hueckel and Baldi (1990). In recent years, constitutive studies based on other frameworks such as hypoplasticity theory (Mašín and Khalili 2012) and different thermodynamic approaches (Bai et al. 2019; Xiao 2014; Zhang and Cheng 2017) have also been carried out for describing the thermo-mechanical behaviour of soils. In this study, the more commonly known and widely used framework of Hueckel and Borsetto (1990) is followed. Before presenting the model, some relevant poineering works in this general framework are reviewed as follows.

Hueckel and Borsetto (1990) extended the modified Cam-clay model by defining the size of the yield surface as a function of temperature as well as volumetric plastic strain. However, it has been found that the thermoplastic deformation at overconsolidated states cannot be well described. To tackle this issue, many subsequent models within the same framework were developed by introducing an additional thermal yield surface (Abuel-Naga et al. 2007a; Cui et al. 2000; Hong et al. 2016), the bounding surface concept (Laloui and Cekerevac 2003; Laloui and François 2009; Robinet et al. 1996; Zhou and Ng 2015), sub-loading surface theory (Yao and Zhou 2013), double hardening mechanism (Liu and Xing 2009), or approximate relationships between the thermally induced plastic strain and OCR (Graham et al. 2001). In addition, as the original and the modified Cam-clay type yield functions tend to significantly overestimate failure stresses on the ‘dry’ side, the Hvorslev surface is often used at the overconsolidated states under non-isothermal conditions (Graham et al. 2001; Yao and Zhou 2013). Many important aspects of the thermomechanical behaviour of saturated clays can be satisfactorily described by these models, and an interesting comparison between some of them was recently provided by Hong et al. (2013).

In addition to the thermal evolutions of the size of the yield surface that was widely studied, some experimental evidence (for example, (Abuel-Naga et al. 2009; Cekerevac and Laloui 2004; Ghahremannejad 2003; Kuntiwattanakul et al. 1995)) showed that the shape of the yield surface may also vary with temperature. To account for the thermal variation of the shape of SBSs, Hueckel et al. (2009) assumed the critical state friction angle of soil to be thermal-dependent. However, this is not consistent with the majority

of existing test data (Cekerevac and Laloui 2004; Hong et al. 2016; Hueckel and Baldi 1990; Mašín and Khalili 2012; Tanaka et al. 1997). While regarding that the slope of the CSL in the p - q space (i.e., M ; q: deviatoric stress) is independent on temperature, the thermal dependency of the shape of SBSs cannot be described by models those relying on the conventional Cam-clay yield functions in the framework of Hueckel and Borsetto (1990). To overcome this limitation, several approaches were attempted in recent years. Abuel-Naga et al. (2009) introduced a temperature related fabric parameter into the modified Cam clay model, which allows the shape of the SBS to vary with temperature. This model focused on the thermo-mechanical behaovuor of soft clays (i.e., on the 'wet' side). Focusing on the isothermal behaivour of saturated clays, Hamidi and Khazaei (2010) and Hamidi et al. (2015) modified the Cam-clay type flow rule with inclusions of temperature effects, and thermal shape flexibility was therefore introduced in the back-integrated yield surfaces. Zhou and Ng (2015) assumed linear variations of the vertical positions of the NCL and the CSL in the v-ln$p$ space with the changes of temperature, respectively. As a result, the shape of the SBS varies with temperature due to the thermal variation of the spacing ratio, adopting the CASM (Clay And Sand Model) yield function proposed by Yu (1995, 1998). As a thermal independent flow rule was adopted, the observed effect of temperature on the plastic flow (e.g., (Abuel-Naga et al. 2009; Cekerevac and Laloui 2004; Hamidi et al. 2015; Uchaipichat and Khalili 2009)) cannot be fully captured by this model.

This paper aims to present an elastoplatic constitutive model for describing the short-term thermomechanical behaviour of both normally consolidated and overconsolidated saturated fine-grain soils. Two yield surfaces are introduced and coupled in the new model. In specific, the mechanical yield surface is defined by extending the isothermal model of CASM with consideration of the temperature effects, and the thermal yield surface is added to describe the thermal induced deformation more realistically, particularly at overconsolidated states. Within the considered temperature range (without freezing or boiling of the pore water), the novelty and usefulness of the new model mainly lie in three aspects:

(a) both the size and the shape of the mechanical yield surface are allowed to vary with temperature. The change in the size is controlled by the preconsolidation pressure that evolves with both thermal and mechanical volumetric plastic strains obeying a newly defined coupling mechanism; the shape variability depends on the thermal dependency

of the spacing ratio, owing to the non-equal shifts of the NCLs and the CSLs when the soil is heated. A nonlinear thermal evolution law for the spacing ratio is defined based on available test observations;

(b) the mechanical behaviour of both normally consolidated and overconsolidated soils at elevated temperatures can be accurately described for both drained and undrained conditions, partly inheriting from the mother model of CASM;

(c) a new thermal dependent non-associated flow rule is proposed and used.

Finally, the proposed model is validated against experimental results of selected element tests in the literature, which include several fine-grained soils and various thermal, stress or combined loading paths such as drained isotropic heating/cooling, drained and undrained triaxial compression tests at elevated temperatures.

State boundary surface

SBS is defined as a boundary of all possible states of a soil element in the *p*-*q*-*v* space (Schofield and Wroth 1968). The NCL represents a trace of the SBS in the *p*-*v* plane, and the yield loci represent its projection in the deviatoric stress plane (i.e. *p*-*q* plane). Constitutive equations can be established by relating the SBS to a family of yield loci in an equivalent two-dimensional stress plane. For example, in Cam-clay models (Roscoe and Burland 1968; Roscoe et al. 1958), the yield surfaces in the *p*-*q* plane are normalised by the preconsolidation pressure which is assumed to evolve with plastic volumetric strains based on the uniqueness of the normalised SBS of isotropically consolidated reconstituted soils at room temperature.

Under non-isothermal conditions, a number of experimental data showed that the NCL moves downwards at elevated temperatures (namely, lower specific volumes at higher temperatures) due to the thermal compaction and NCLs at different temperatures are almost parallel to each other (Abuel-Naga et al. 2007b; Burghignoli et al. 1992; Campanella and Mitchell 1968; Di Donna and Laloui 2015). Similar downward shifts of the CSLs were observed (Cekerevac and Laloui 2004; Graham et al. 2001). Meanwhile, although exception was reported (Cekerevac and Laloui 2004), a majority of experimental data showed that the NCL may remain parallel to the CSL for reconstituted soils at different temperatures (e.g., Fig. 1) (Ghahremannejad 2003; Graham et al. 2001; Lingnau et al. 1995; Tanaka 1995), and this was commonly accepted as a fundamental hypothesis

in many thermomechanical soil models based on the critical state theory (e.g., (Cui et al. 2000; Graham et al. 2001; Hueckel and Borsetto 1990; Seneviratne et al. 1993; Zhou and Ng 2015)).

Based on the above findings, the effects of temperature on the preconsolidation pressure ($p_{c(\mathrm{T})}$) and the corresponding critical state stress ($p_{x(\mathrm{T})}$) are illustrated in Fig. 2. These two representative pressures are often correlated by the spacing ratio of NCL and CSL, that is $r_{(\mathrm{T})} = p_{c(\mathrm{T})} / p_{x(\mathrm{T})}$ (Wroth 1984). At a constant plastic strain condition (i.e., on the same swelling line), $p_{c(\mathrm{T})}$ and $p_{x(\mathrm{T})}$ become smaller at higher temperatures as the NCL and CSL shift downwards in the *v*-*p* plane, respectively. As a result, the SBS shrinks when the soil is heated (Mašín and Khalili 2012). Thermal evolutions of the NCL and the CSL are not necessarily always the same (Cekerevac and Laloui 2004; Ghahremannejad 2003; Kuntiwattanakul et al. 1995; Tanaka et al. 1997; Uchaipichat and Khalili 2009), which thus leads the spacing ratio to be temperature dependent.

In standard Cam-clay models, the same spacing ratio values are used for all soil types (namely, 2.718 and 2 for the original and the modified Cam-clay models, respectively (Wroth 1984; Yu 1998)) although in reality this is not always the case. In particular, while the standard Cam-clay yield curves (normalised by $p_{c(\mathrm{T})}$) are used directly in non-isothermal conditions, the aforementioned temperature dependency of the spacing ratio cannot be accounted for. Instead, it is very convenient to introduce the general stress-state relationship proposed by Yu (1998), namely:

$$\left(\frac{\eta}{M}\right)^n = 1 - \frac{\xi_{(\mathrm{T})}}{\xi_{R(\mathrm{T})}} \qquad (1)$$

where $\eta = q / p$, is the stress ratio. n is a material constant, which controls the curvature of the yield surface and typically ranges between 1.0-5.0. $\xi_{(\mathrm{T})}$ represents 'the state parameter' (Been and Jefferies 1985; Yu 1998). $\xi_{R(\mathrm{T})}$ is a reference parameter, which represents the vertical distance between the NCL and the CSL at a given temperature and equals $(\lambda - \kappa)\ln r_{(\mathrm{T})}$ (Fig. 2).

$$\xi_{(\mathrm{T})} = v + \lambda \ln p - \Gamma_{(\mathrm{T})} \qquad (2)$$

where $v = 1 + e$, and e is the void ratio; $N_{(T)}$ and $\Gamma_{(T)}$ denote the specific volumes of the temperature-dependent NCL and CSL at $p = 1\text{kPa}$, respectively. λ and κ are the slopes of the NCL (or CSL) and the swelling line in the v-ln p space (see Fig. 2), respectively.

For fine-grained soils, the overconsolidation ratio (OCR=$p_{c(T)} / p$) is more often used to define the soil state. As depicted in Fig. 2, eq.(2) can be equivalently expressed as:

$$\xi_{(T)} = (\lambda - \kappa) \ln\left(\frac{r_{(T)}}{\text{OCR}}\right) \tag{3}$$

It is important to note that OCR= $r_{(T)}$ (or $\xi_{(T)}$ =0) at the critical state; OCR< $r_{(T)}$ on the 'wet' side (i.e., soft clay, $\xi_{(T)}$ >0); OCR> $r_{(T)}$ on the 'dry' side (i.e., stiff clay, $\xi_{(T)}$ <0).

It is clear that in eq.(1) the spacing ratio is allowed to vary with material type and temperature. In other words, the SBS is generalised to accommodate the complex thermal-dependent behaviour of various soils, providing a link between classical critical state soil mechanics and thermomechanical constitutive modelling. By normalising eq.(1) with the preconsolidation pressure, a generalised yield surface in the p-q plane is obtained as:

$$f^{\text{MY}} = \left(\frac{q}{Mp}\right)^n + \frac{\ln(p / p_{c(T)})}{\ln r_{(T)}} \tag{4}$$

The yield function of the original Cam-clay model can be recovered exactly by choosing n=1 and $r_{(T)}$=2.718, and the 'wet' side of the modified Cam clay model can be matched accurately by choosing $r_{(T)}$=2 in conjunction with a suitable value of n (typically around 1.5–2) in eq.(4). In agreement of the majority of the published experimental data (e.g., (Cekerevac and Laloui 2004; Hong et al. 2016; Hueckel and Baldi 1990; Tanaka et al. 1997)), M is assumed to be temperature-independent in the present model. The material constant n is also assumed to be independent of temperature. In eq.(4), thermal variations of the SBS (size and shape) are controlled by thermal evolutions of the preconsolidation pressure (i.e., $p_{c(T)}$) and the spacing ratio (i.e., $r_{(T)}$), and they will be defined in the next section. It needs to be pointed out that conflict results with regard to the dependencies of M and n on the temperature were reported for some particular soils

(Hamidi et al. 2015; Hueckel and Pellegrini 1991). However, this is not taken into account in the present basic model due to the lack of compelling evidence.

Thermo-elastoplastic modelling

Assuming compressive stress and strain as positive, two stress variables normally used in critical state soil mechanics are defined as:

(5 a, b) $$p = \sigma_{ii}/3 = (\sigma_{11}+\sigma_{22}+\sigma_{33})/3 \quad , \quad q = \sqrt{3(\sigma_{ij}-p\delta_{ij})(\sigma_{ij}-p\delta_{ij})/2}$$

where σ_{ij} is principal effective stress tensor; δ_{ij} is the Kronecker delta. For notation convenience, all stress variables in this paper are effective values.

The volumetric and deviatoric strain increments are defined as:

(6 a, b) $$\mathrm{d}\varepsilon_{\mathrm{v}} = \mathrm{d}\varepsilon_{11}+\mathrm{d}\varepsilon_{22}+\mathrm{d}\varepsilon_{33} \quad ,$$

$$\mathrm{d}\varepsilon_{\mathrm{d}} = \frac{2}{3}\sqrt{(\mathrm{d}\varepsilon_{11}-\mathrm{d}\varepsilon_{22})^2+(\mathrm{d}\varepsilon_{11}-\mathrm{d}\varepsilon_{33})^2+(\mathrm{d}\varepsilon_{33}-\mathrm{d}\varepsilon_{22})^2}$$

where ε_{v} and ε_{d} denote the volumetric and deviatoric strains, respectively. ε_{ii} are principal strain components. The total strain increments are split into elastic and plastic components (i.e., $\mathrm{d}\varepsilon_{\mathrm{v}} = \mathrm{d}\varepsilon_{\mathrm{v}}^{\mathrm{e}} + \mathrm{d}\varepsilon_{\mathrm{v}}^{\mathrm{p}}$ and $\mathrm{d}\varepsilon_{\mathrm{d}} = \mathrm{d}\varepsilon_{\mathrm{d}}^{\mathrm{e}} + \mathrm{d}\varepsilon_{\mathrm{d}}^{\mathrm{p}}$), which depend on both mechanical and thermal loadings. They are treated separately in the small deformation domain as below. Note that heating and/or cooling of the soil are assumed to be under drained conditions in this paper.

Elastic behaviour

For elastic deformation, it is common to assume that temperature changes only induce elastic volumetric strain in soils (Abuel-Naga et al. 2007a; Cui et al. 2000; Hueckel and Borsetto 1990; Laloui and François 2009; Yao and Zhou 2013). In other words, the elastic deviatoric strain is solely associated with mechanical loading. As a result, the thermoelastic strain increments can be defined as:

(7) $$\mathrm{d}\varepsilon_{\mathrm{v}}^{\mathrm{e}} = \frac{\kappa}{1+e}\frac{\mathrm{d}p}{p} - \alpha \mathrm{d}T$$

(8) $$\mathrm{d}\varepsilon_{\mathrm{d}}^{\mathrm{e}} = \frac{2(1+\mu)}{9(1-2\mu)}\frac{\kappa}{1+e}\frac{\mathrm{d}q}{p}$$

where μ is Poisson's ratio, and it is assumed to be constant for a given soil. α is the drained elastic volumetric thermal expansion coefficient. It was shown that α may essentially be considered as independent of stress state and temperature (Cui et al. 2000; Hong et al. 2013; Mašín and Khalili 2012; Sultan et al. 2002). Therefore, a constant value of α is assumed in the eq.(7).

In eqs.(7) and (8), the mechanically induced strains are described by using the hypoelastic model as in Cam-clay models (Wood 1990). Although thermal dependent κ has been reported (Eriksson 1989; Graham et al. 2001), many results showed that the slope of the swelling line (κ) is temperature independent (Abuel-Naga et al. 2007b; Campanella and Mitchell 1968; Cui et al. 2000). It was argued by Abuel-Naga et al. (2007b) that this discrepancy is due to the difference in the test procedure, and a constant value of κ is preferable for defining the mechanical elastic behaviour within the yield limit. This is adopted in the present model. It needs to be pointed out that thermal variations of κ, if any, would lead to additional changes to the critical state stress than that is purely caused by thermal shift of the CSL, and thereby could further alter the shape of the SBS (Tanaka 1995).

Thermomechanical yield curves

In the framework of elastic-plastic theory, thermomechanical yield curves describe the boundary of a thermoelastic domain, within which reversible deformation occurs due to changes of temperature or effective stresses or both. In this model, similar to Cui et al. (2000) and Abuel-Naga et al. (2007a), two yield surfaces are introduced in the *p*-*T* plane, namely mechanical yield (MY) surface and thermal yield (TY) surface. The former one corresponds to the thermal evolution of the SBS in the *p*-*q* space, and the latter mechanism is for describing the thermally induced volume change of soil more realistically.

(a) Mechanical yield limit

The mechanical yield surface in the *p*-*q* space was defined in eq.(4). Subjected to temperature changes, the size of the SBS varies due to the thermal evolution of the preconsolidation pressure (i.e., $p_{c(T)}$) (Cui et al. 2000; Hueckel and Borsetto 1990; Laloui and Cekerevac 2003; Wang et al. 2016). Several evolution laws of $p_{c(T)}$ in response to temperature changes at constant plastic strain (i.e. at no heat-induced plastic strain) were proposed in the *p*-*T* plane (Hueckel and Borsetto 1990; Laloui and Cekerevac 2003;

239 Moritz 1995). Based on available experimental data of a variety of soils, Moritz (1995)
240 and Wang et al. (2016) demonstrated that it is reasonable to assume a linear relationship
241 between $\ln\left(p_{c(T)} / p_{c(T_0)}\right)$ and $\ln\left(T / T_0\right)$, that is

242 (9) $$\ln\left(\frac{p_{c(T)}}{p_{c(T_0)}}\right) = \theta \ln\left(\frac{T_0}{T}\right)$$

243 where $p_{c(T_0)}$ is the preconsolidation pressure at reference (or room) temperature T_0; θ is
244 a material parameter that determines the thermal dependence of the preconsolidation
245 pressure. With a positive value of θ, eq.(9) predicts a nonlinear decrease of $p_{c(T)}$ with
246 temperature increases (e.g. Fig. 3).Wang et al. (2016) validated this relationship with
247 seven types of clays and also pointed out that eq.(9) in fact is the first-order approximation
248 of the dependency law of Laloui and Cekerevac (2003).

249 Meanwhile, the shape of the SBS may also change with temperature (Abuel-Naga et
250 al. 2009; Hamidi et al. 2015; Hong et al. 2016; Hueckel et al. 2009; Mašín and Khalili
251 2012; Zhou and Ng 2015). This thermal variation may be attributed to the thermally
252 induced irreversible changes of soil structure (fabric) (Abuel-Naga et al. 2009; Zymnis et
253 al. 2018), and it can be captured by allowing the spacing ratio (i.e., $r_{(T)}$) in the yield
254 function to be temperature dependent. As shown in Fig. 2, $\ln\left(p_{c(T)} / p_{c(T_0)}\right)$ is the
255 horizontal distance between the NCLs at T_0 and elevated temperature T, respectively, at a
256 constant plastic strain condition. It is assumed that the translation of the CSL due to
257 temperature changes is similar to that of the NCL. Therefore, by definition, the thermal
258 variation of the spacing ratio can be expressed as:

259 (10) $$\ln\left(\frac{r_{(T)}}{r_{(T_0)}}\right) = \zeta \ln\left(\frac{T_0}{T}\right)$$

260 where $r_{(T_0)}$ denotes the spacing ratio at the reference temperature T_0; ζ is a constant value
261 which controls the thermal variation of the spacing ratio. The influence of the thermal
262 evolution of $r_{(T)}$ on the yield surface is illustrated in Fig. 3. According to eqs.(9) and (10),
263 the horizontal translation of the CSL due to the temperature change of (T-T_0) (i.e.,
264 $\ln\left(p_{x(T)} / p_{x(T_0)}\right)$) equals $(\theta - \zeta)\ln\left(T_0 / T\right)$. As the CSL may stay or move downwards in

265 the v-ln p space when the soil is heated (Abuel-Naga et al. 2007b; Cekerevac and Laloui
266 2004; Ghahremannejad 2003; Kuntiwattanakul et al. 1995; Tanaka et al. 1997), $\zeta \le \theta$
267 and ζ could be positive, zero, or negative, which indicates that the parallel shift of the
268 CSL is smaller, the same, or greater than that of the NCL with the same temperature
269 change. For example, compred to the experimental data of Ghahremannejad (2003) (refer
270 to Fig. 1), Fig. 4 shows that eq.(10) with with ζ=0.082 agrees well with the measured
271 results; on the contrary, a negative value of ζ (see Table 1) was calibrated from results of
272 drained triaxial tests that were performed by Uchaipichat and Khalili (2009) on Bourke
273 silt at different temperatures as detailed later.

274 (b) Thermal yield limit

275 Upon drained heating, the volume change of soil greatly depends on the stress history
276 (e.g., OCR). For example, with rising temperature, thermal contraction dominates at low
277 values of OCR, whereas the soil may dilate first and then transit to contract at intermediate
278 OCRs. The transition temperature from expansion to contraction increases with higher
279 OCR values (Abuel-Naga et al. 2007a; Baldi et al. 1988; Cekerevac and Laloui 2004; Cui
280 et al. 2000; Sultan et al. 2002; Towhata et al. 1993). At very high OCRs, the soil may
281 only experience thermal expansion in the temperature range without freezing or boiling
282 of the pore water. Based on elastoplastic theory, the reversible thermal expansion is
283 attributed to thermoelastic deformation (e.g., eq.(7)), and the thermal contraction is
284 interpreted as thermoplastic (Hueckel and Baldi 1990). It was reported that the transition
285 temperature for overconsolidated soils is generally much lower than the yield limit
286 predicted by the MY curve even though the thermal evolution of the preconsolidation
287 pressure is considered (Abuel-Naga et al. 2007a; Coccia and McCartney 2016). Cui et al.
288 (2000) proposed that this phenomenon can be captured by introducing a second yield
289 curve (i.e., TY) in the p-T plane. Here, the TY curve proposed by Abuel-Naga et al.
290 (2007a) (i.e., eq.(11)) is followed.

291 (11) $$\frac{p_{c(T_0)}}{p_{T(T)}} = \beta\sqrt{\ln\frac{T}{T_0}} + 1$$

292 Then the TY function can be written as

293 (12) $$f^{TY} = p_{T(T)}\left(\beta\sqrt{\ln\frac{T}{T_0}} + 1\right) - p_{c(T_0)} = 0$$

where $p_{T(T)}$ is the effective stress at the aforementioned transition temperature; β is the evolution parameter depending on the loading history, and its initial value is β_0. Fig. 4 shows example results calculated by eq.(11) with different fixed values of β in the p_T-T plane, under stresses below which the deformation is assumed to be thermoelastic. The adopted TY curve coincides with the MY curve at room temperature, which is in agreement with experimental observations (Abuel-Naga et al. 2007a).

Thermomechanical plastic strains

Mechanical plastic volumetric strain (ε_v^{mp}) is produced when the mechanical yield limit is reached. Following the conventional soil plasticity theory, mechanical plastic strain increments can be expressed as

$$\text{(13 a,b)} \qquad d\varepsilon_v^{mp} = d\lambda_m \frac{\partial g^{MY}}{\partial p} \ , \ d\varepsilon_d^{mp} = d\lambda_m \frac{\partial g^{MY}}{\partial q}$$

where $d\lambda_m$ is the plastic multiplier, a positive scalar. g^{MY} is the plastic potential function corresponding to mechanical loading. ε_d^{mp} is the plastic deviatoric strain due to mechanical loading, and $\varepsilon_d^{p} = \varepsilon_d^{mp}$ as no plastic deviatoric strain is induced by thermal loading.

Although the conventional Cam-clay type flow rules were often used directly at elevated temperatures (Cui et al. 2000; Graham et al. 2001; Laloui and François 2009; Zhou and Ng 2015), it was shown that changes of the temperature may also affect the plastic flow rule (Abuel-Naga et al. 2007b; Hamidi et al. 2015). Hence, a simple thermal dependent flow rule is proposed in eq.(14) by slightly modifying the conventional Cam-clay type flow rule (Hong et al. 2016; McDowell and Hau 2003). Inspired by some experimental observations (Abuel-Naga et al. 2009; Hamidi et al. 2015; Uchaipichat and Khalili 2009), $k = 2\ln r_{(T)}$ is assumed by simplifying the general stress-dilatancy relation proposed by Yu (2006).

$$\text{(14)} \qquad \frac{d\varepsilon_v^{mp}}{d\varepsilon_d^{mp}} = \frac{M^2 - \eta^2}{k\eta}$$

Then the non-associate plastic potential function g^{MY} can be readily obtained by integrating eq.(14) (Yu 2006) as

$$g^{\mathrm{MY}} = k\ln\left[1+(k-1)\left(\frac{\eta}{M}\right)^{2}\right]+2(k-1)\ln\left(\frac{p}{C}\right) \quad (15)$$

where C indicates the size of the plastic potential surface, which can be determined by solving the above equation for any given stress state. It is noted that the potential function with $k=2$ corresponds to the modified Cam-clay model.

In eq.(14), the flow rule is related to the temperature dependent spacing ratio. While ζ is positive, zero, or negative, the incremental plastic strain ratio (i.e., $\mathrm{d}\varepsilon_{\mathrm{v}}^{\mathrm{mp}}/\mathrm{d}\varepsilon_{\mathrm{d}}^{\mathrm{mp}}$) increases (Abuel-Naga et al. 2007b), remains unchanged (Graham et al. 2001), or decreases (Uchaipichat and Khalili 2009) with temperature increases, which coincides with experimental observations in the literature. For example, in soft Bangkok clay, Abuel-Naga et al. (2007b) observed that the NCL move downwards while the CSL almost remain unaltered when the soil is heated. Therefore, ζ is positive and close to the value of θ (e.g., Table 1). With a positive value of ζ, eq.(14) predict that $\mathrm{d}\varepsilon_{\mathrm{v}}^{\mathrm{mp}}/\mathrm{d}\varepsilon_{\mathrm{d}}^{\mathrm{mp}}$ increases as temperature rises, which is consistent with the test observation (Fig. 6). Note that underestimation of the temperature effect is shown at high stress ratios. This can be alleviated by involving in several additional model parameters (Hamidi et al. 2015). However, this was not attempted in this study to keep the model consistent and simple.

Then, the plastic multiplier $\mathrm{d}\lambda_{\mathrm{m}}$ can be determined from the consistency condition of the MY function, as follows:

$$\mathrm{d}\lambda_{\mathrm{m}} = -\left(\frac{\partial f^{\mathrm{MY}}}{\partial p}\mathrm{d}p+\frac{\partial f^{\mathrm{MY}}}{\partial q}\mathrm{d}q+\frac{\partial f^{\mathrm{MY}}}{\partial T}\mathrm{d}T\right)\Bigg/\frac{\partial f^{\mathrm{MY}}}{\partial p_{c(\mathrm{T}_0)}}\frac{\partial p_{c(\mathrm{T}_0)}}{\partial \varepsilon_{\mathrm{v}}^{\mathrm{mp}}}\frac{\partial g^{\mathrm{MY}}}{\partial p} \quad (16)$$

Upon heating, thermal plastic contraction occurs when the TY limit is reached. Experimental results (for example, (Abuel-Naga et al. 2007a; Baldi et al. 1991; Laloui and François 2009; Sultan et al. 2002)) indicated that the thermally induced plastic volumetric strain highly depends on the OCR value in addition to temperature changes (Cui et al. 2000; Graham et al. 2001; Hong et al. 2016; Yao and Zhou 2013). And Demars and Charles (1982) and Sultan et al. (2002) reported that the thermal plastic volumetric strain ($\varepsilon_{\mathrm{v}}^{\mathrm{tp}}$) is independent of the magnitude of the effective confining stress applied.

According to these findings, eq.(17) with only one additional material parameter is proposed and used to predict ε_v^{tp}.

$$(17) \qquad d\varepsilon_v^{tp} = \omega\left(T - T_0\right)\left(\frac{p}{p_{c(T_0)}}\right)^2 dT$$

where ω is a soil parameter controlling the development of ε_v^{tp} and is assumed to be constant. Eq.(17) is triggered only while the TY surface (eq.(12)) is reached. In eq.(17) the hardening/softening of $p_{c(T_0)}$ is involved (e.g., eq.(18)). Together with eq.(9), it can be seen that the thermally induced plastic volumetric strain defined here is a function of the temperature change and the current soil stress state (i.e., OCR), which is consistent with the abovementioned literature. Excellent agreement is shown in Fig. 7 between predicted and measured results of ε_v^{tp} for different soils at various stress conditions, which directly confirms the rationality of eq.(17).

Thermomechanical hardening laws and coupling mechanism

The preconsolidation pressure $p_{c(T_0)}$ appears in both the mechanical (i.e., eqs.(4) and (9)) and the thermal yield functions (i.e., eq.(12)) as a hardening parameter. It is postulated that $p_{c(T_0)}$ depends on the total plastic volumetric strains (ε_v^p) as defined in eq.(18), and, thus, these two plastic mechanisms are coupled through ε_v^p. Mechanical and thermal plastic volumetric strains will move the mechanical and thermal yield limits simultaneously.

$$(18) \qquad dp_{c(T_0)} = p_{c0(T_0)} \frac{1+e_0}{\lambda - \kappa} d\varepsilon_v^p$$

$$(19) \qquad d\varepsilon_v^p = d\varepsilon_v^{tp} + d\varepsilon_v^{mp}$$

where $p_{c0(T_0)}$ is the initial preconsolidation pressure at the reference temperature T_0.

The volumetric hardening (i.e., eq.(18)) mainly affects the sizes or positions of the MY and TY curves. Meanwhile, the shapes of them may also vary with temperature due to thermal evolutions of the stress pacing ratio (see eq.(10)) and the parameter β. While the TY mechanism is activated, a hardening phenomenon moves the TY surface upwards in

the T-p plane as β reduces (see Fig. 5). The evolution of β can be determined from the consistency condition of TY function, as follows:

$$\mathrm{d}f^{\mathrm{TY}} = \frac{\partial f^{\mathrm{TY}}}{\partial p}\mathrm{d}p + \frac{\partial f^{\mathrm{TY}}}{\partial T}\mathrm{d}T + \frac{\partial f^{\mathrm{TY}}}{\partial \beta}\mathrm{d}\beta + \frac{\partial f^{\mathrm{TY}}}{\partial p_{c(\mathrm{T}_0)}}\mathrm{d}p_{c(\mathrm{T}_0)} = 0 \quad (20)$$

Mechanical plastic strains will develop when the MY mechanism is activated as defined in eqs.(13 a,b), and thermal plastic volumetric strains will be induced due to temperature changes as defined in eq.(17). In this model, the thermomechanical soil response is loading path dependent. For example, although the TY curve will not be activated upon purely isothermal loading in the proposed model, thermal evolutions of the preconsolidation pressure and the spacing ratio possibly occurred during pre-thermal loadings. As a result, the isothermal strength of soil may either increase or decrease, depending on the stress and temperature history. For illustration, thermal evolutions of the MY and TY curves are discussed in the p-T plane along three typical drained thermal loading paths (e.g., from T_0 to T in Fig. 8) as follows:

(a) Loading path: OABC. For heavily overconsolidated soils (e.g., point B), only recoverable thermal expansion occurs upon heating within the concerned temperature range (e.g., path B→C). As the elastic thermal expansion coefficient α was assumed to be constant in eq.(7), the soil volume increases or decreases linearly during drained heating or cooling (e.g., Fig. 8 (a)). As no plastic volumetric strain will be produced along this typical path, the preconsolidation pressure reduces at higher temperatures as defined by eq.(9).

(b) Loading path: OADEF. At point D, the soil is intermediately overconsolidated. Upon heating from room temperature, thermal expansion dominates before reaching the TY limit (i.e., path D→E in Fig. 8 (b)). Afterwards, thermal plastic deformation develops beyond the transition temperature (i.e., point E), and, therefore, $p_{c(\mathrm{T}_0)}$ evolves. As thermal plastic deformation accumulates, a reduction of the soil volume will be caused (e.g., Fig. 8 (c)). Overall, along with the path D→E→F, thermal expansion occurs first, followed by contractions. The transition temperature gets higher with greater OCR values as that has been widely observed in soil heating tests (Abuel-Naga et al. 2007b; Baldi et al. 1988; Cekerevac and Laloui 2004; Sultan et al. 2002).

(c) Loading path: OAGH. At point A (normally consolidated state at room temperature), the proposed MY and TY coincides, and both of them are reached immediately. Upon heating from point A, $p_{c(T_0)}$ evolves as both plastic strain hardening and thermal softening occur, and, therefore, the locations of the MY and TY curves move as defined by eqs. (9) and (12), respectively. It is found that both the TY and MY limits will be reached along the heating path from A to G in the coupled hardening mechanism defined. Thus, both thermal and mechanical plastic strains develop, and the consistency conditions of eqs.(16) and (20) must be satisfied simultaneously. From G to H, the soil contraction is solely caused by thermal plastic deformation as only the TY mechanism is triggered. In other words, the soil always stays as normally consolidated under thermal loading in the temperature range between T_A and T_G (temperatures at points A and G, respectively), which is consistent with the test observation of Plum and Esrig (1969) in heating tests on Newfield clay from 24°C to 50°C; thermally induced overconsolidation effect is predicted with further temperature rise as the TY limit is always reached prior to the MY limit along G to H, which agrees well with experimental observations (Abuel-Naga et al. 2007a; Burghignoli et al. 1992; Sultan et al. 2002). As a result, an *s*-shape *T*-ε_v curve is predicted by the present model as illustrated in Fig. 8 (f). The range of path A →G might be soil-specific (Sultan et al. 2002).

Determination of model parameters

There are a total number of 12 parameters required in the proposed model. The isothermal parameters (λ, κ, M, μ, $\Gamma_{(T)}$, n, and $r_{(T)}$) are similar to those of the mother model of CASM, the first five of which are common soil parameters of Cam-clay models. The determination procedure and typical values of them were elaborated by Yu (1998). Under non-isothermal conditions, $r_{(T)}$ and $\Gamma_{(T)}$ were assumed to be temperature-dependent, which can be calculated by eqs.(10) and (21), respectively.

$$\Gamma_{(T)} = \Gamma_{(T_0)} - (\lambda - \kappa)(\theta - \zeta)\ln\left(T / T_0\right) \quad (21)$$

New soil parameters that are introduced to account for the temperature effects include α, θ, ζ, β_0, and ω. The role of each of them and practical methods for determining them are briefly discussed as follows.

(a) The elastic thermal expansion coefficient α can be calibrated from the cooling stage of a drained heating-cooling test or a drained heating test on a heavily overconsolidated soil in the T-ε_v plot. α is mainly determined by the thermal expansion coefficient of the solid constituent (Khalili et al. 2010) and can be considered as constant in the order of 10^{-5}°C^{-1} for most practical purposes.

(b) As defined in eq.(9), θ controls the temperature dependency of the preconsolidation pressure at a constant plastic strain, which is generally of positive value. It can be obtained by performing two or more isotropic compression tests at different constant temperatures.

(c) β_0 determines the initial shape or position of the TY curve in the p-T plot (e.g., Fig. 5). The transition temperature at a given OCR can be determined by plotting isotropic drained heating test results in the ε_v-T plot (e.g., Fig. 8 (c)). With measured values of the transition temperature at different OCRs (at least two), β_0 can be fitted using eq.(11).

(d) The spacing ratio typically lies in the range of 1.5~3.0 for clays (Yu 1998), which can be determined by locating the NCL and the CSL at a given temperature. The thermal evolution of $r_{(T)}$ is controlled by the parameter ζ as defined in eq.(10). With measured values of $r_{(T)}$ at different temperatures (at least two), ζ can be obtained by the method of fitting in the $r_{(T)}$-T plot (e.g., Fig. 3). Alternatively, as the spacing ratio defines the shape of the MY surface, the relationship between $r_{(T)}$ and T can also be estimated by fitting the yield loci obtained at different temperatures.

(e) In eq.(17), ω controls the development of thermal plastic strain. It can be calibrated from thermal isotropic drained heating tests (e.g., Fig. 7).

In the above procedure, both 1D compression and 3D triaxial tests at a range of temperatures are involved to determine the soil parameters. Alternatively, the whole set of parameters can be efficiently identified with a limited number of 3D conventional soil tests (e.g. triaxial tests at different temperatures) using an appropriate optimization method (Jin et al. 2017; Mattsson et al. 1999; Yin et al. 2017). In general, the optimization procedure consists of two core parts: (1) the definition of an error function measuring the difference between model responses and experimental results and (2) the selection of an optimization strategy to enable the search for the minimum of this error function (Yin et al. 2018).

Evaluation of the proposed model

To test the reliability of the proposed model, predictions of various short-term thermomechanical behaviour of soils are compared with experimental data published in the literature. Note that the simulations of these soil element tests were performed at the element level, namely the distributions of strains and temperature were regarded as uniform throughout the soil element. Model parameters for each soil were calibrated following the above procedure based on test data, and they are summarised in Table 1.

Temperature effect on the drained volumetric behaviour

Thermally induced volume changes of natural Boom clay and reconstituted Bangkok clay subjected to heating-cooling cycles at different OCRs were simulated, and they are compared with experimental results of Baldi et al. (1991) and Abuel-Naga et al. (2007a) in Fig. 9. In the tests of Baldi et al. (1991), the Boom clay was saturated under a constant p=2MPa first, then isotropically loaded up to 4 MPa, and unloaded to 1 MPa prior to heating. After, three heating-cooling cycles of 21.5-95-21.5 °C was applied under p=1, 3, 6 MPa (OCR=4, 1.33, 1, respectively) with a continuous test procedure as depicted in Fig. 9 (a). The adopted tests of Abuel-Naga et al. (2007a) (Fig. 9 (b)) were performed in a similar manner. The soil samples were consolidated under a vertical stress of 200 kPa and unloaded to be different stress levels (giving OCR=1, 2, 4, and 8), followed by an incremental heating-cooling cycle of 22-90-22 °C.

Taking the tests of Baldi et al. (1991) as an example, the thermal related parameters α, β_0, and ω were calibrated based on the data during the heating stage at p=1MPa; θ=0.24 was determined as the preconsolidation pressures were 6 MPa and 4.2 MPa at 21.5°C and 95°C, respectively; other parameters were measured by Baldi et al. (1991) as summarised in Table 1. Note that two methods were used to calculate the drained thermal volumetric strain in the test. The results that subtracted the thermal expansion of both the pore water and the solid phase from the measured volume of water expelled from the soil sample were used in Fig. 9 (a) because they are believed more accurate as discussed by Hong et al. (2013). Overall, great effects of stress history on the thermal volumetric strain under drained heating-cooling cycles are shown in Fig. 9, and the predicted and measured results were in good agreement at different OCRs. This demonstrates the model capacity in capturing these effects, and the mechanisms were elaborated in Fig. 8.

Fig. 10 shows a comparison between simulated and measured results of Bangkok clay on a combined thermomechanical path. The test consists in oedometric loading of the normally consolidated Bangkok clay until an effective vertical stress of 100 kPa, followed by a heating-cooling cycle of 22-90-22°C and finishing at vertical loading up to 200 kPa. (Abuel-Naga et al. 2007a). An apparent overconsolidation state after one heating-cooling cycle was caused, which is in line with other observations in the literature (for example, (Burghignoli et al. 1992; Sultan et al. 2002)). Using the soil parameters in Table 1, this thermally induced overconsolidation behaviour is also well predicted by the proposed model (Fig. 10).

Undrained triaxial compression tests at different temperatures

Tanaka (1995) reported several undrained triaxial compression tests on reconstituted Illite clay at different temperatures. In the tests, three normally consolidated specimens were prepared by increasing the effective consolidation pressure to 1.5 MPa at T_0=28°C; two overconsolidated specimens were produced by applying an effective consolidation pressure up to 1MPa followed by isotropic unloading to 0.5 MPa, giving OCR=2. After initial consolidations, the specimens were heated to desired temperatures under drained conditions. Finally, undrained triaxial shear tests were performed with the normally consolidated specimens at three constant temperatures (i.e., 28°C, 65°C and 100°C) and with the overconsolidated specimens at two constant temperatures (i.e., 28°C and 65°C). The calibrated model parameters are listed in Table 1. It should be noted that the stress-state coefficient n and the spacing ratio were obtained by fitting the measured yield limits on the 'wet' side as shown in Fig. 11; $\omega=0.6\times10^{-6}/°C^2$ was fitted with the experimental results on the normally consolidated sample at T=65°C; typical values of α and β_0 were assumed as related data of thermal isotropic tests were not available in the reference.

Numerical simulations were performed following the same loading paths as those were applied in the tests. Good agreement between the measured and predicted stress-strain curves is shown in Fig. 12. The results show that the normally consolidated Illite clay has greater undrained shear strength and generated lower pore water pressures at higher temperatures, and the difference becomes smaller for samples of OCR=2. The predicted yield loci in Fig. 11 indicate that the peak shear strength at higher OCRs may turn to decrease with increases of temperature, and this has also been observed in similar test on different soils (De Bruyn and Thimus 1996; Hueckel and Borsetto 1990). The predicted

and measured stress paths of the normally consolidated soil samples at different temperatures are compared in Fig. 13. Apparent thermal overconsolidation behaviour at elevated temperatures are shown due to the thermal evolution of the mechanical yield surface as explained in Fig. 8 (e.g. path OAGH). As the soil response is assumed as purely elastic within the SBS (i.e., elastic wall) in the present model, which is described by using a simple hypoelastic model (i.e., eqs.(7) and (8)), the predicted transition from elastic to elastoplastic states is unnecessarily abrupt. This issue can be readily tackled by introducing the bounding surface scheme (Dafalias 1986; Laloui and François 2009; Zhou and Ng 2015) or empirical relationships accounting for soil stiffness degradation (Hardin and Black 1968; Vardanega and Bolton 2013). Meanwhile, this will also give a closer prediction of the stress path for the test at 100°C. In order to minimise the number of model parameters, they were not included in this basic model.

It is shown in Fig. 12 that, for normally consolidated specimens at elevated temperatures, the peak deviatoric stresses are slightly underestimated, and excess pore water pressures (Δu) are therefore over-predicted. In the framework of critical state soil mechanics, no further volumetric plastic strains will be generated at the critical state. Hence, constant critical-state values of q and Δu were predicted by soil models with the volumetric hardening mechanism only, which agree well with the test results at room temperature (e.g., T=2.8°C in Fig. 13). However, as shown in Fig. 13, hardening continued at the critical state for the specimens at elevated temperatures, and the hardening effect was more significant at T=100°C. This phenomenon may be related to thermally induced anisotropy due to the heterogeneity of clay. However, it is important to note that the finding on this temperature-related hardening phenomenon at the critical state is not conclusive in the literature, for example, an opposite trend was reported by Abuel-Naga et al. (2007b) in undrained triaxial tests on soft Bangkok clay. In theory, it is anticipated that this behaviour can be modelled by adopting more complex hardening laws with an inclusion of additional contributions from plastic shear strains (e.g., combined deviatoric and volumetric hardening laws) (Collins and Kelly 2002; Dafalias and Taiebat 2013; Wheeler et al. 2003; Yu et al. 2005).

Drained triaxial compression tests at different temperatures

Drained triaxial compression tests on saturated Bourke silt at different temperatures reported by Uchaipichat and Khalili (2009) were simulated and compared in Figs. 14 and 15. Nine soil specimens were initially consolidated under an isotropic loading of 200 kPa

at 25°C, followed by unloading to 150 kPa, 100 kPa or 50 kPa (i.e., OCR=1.33, 2, 4). Then some of them were heated to 40°C or 60°C under drained condition prior to performing isothermal drained triaxial compression tests. Note that the model parameters α, β_0 and ω were determined by fitting the results of OCR=2 at T=40°C; n, $r_{(T)}$, and ζ were calibrated by fitting the measured yield loci as shown in Fig. 14. Note that the yield points at high values of OCR are underestimated, and this directly leads to underestimations of the peak strength for tests at OCR=4 (Fig. 14 (c)).

For the Bourke silt, it was measured that the spacing ratio increases with an increase in temperature (e.g., Fig. 14). This behaviour is also reflected in the plot of volumetric strain versus shear strain (e.g., Fig. 14 (c)). It is shown that the amount of shear dilation of soil at OCR=4 (strain softening) is smaller at higher temperatures, and this can be well captured by the proposed flow rule (eq.(14)) with a negative value of ζ. In the drained triaxial shear tests of the Bourke silt (Fig. 14), the shear stress reduces with the increase of the temperature before reaching the critical state, where the temperature effects on the stress path almost vanish. On the contrary, the temperature effects on the volumetric strain accumulate with shear strain, and the soil deformation becomes more contractive at a higher temperature. Although the volumetric strains at OCR=1.33 and the peak strength at OCR=4 were underestimated slightly, overall soil behaviours are well reproduced by the model simulations, which confirms the validity of the proposed model for drained triaxial shear tests at different temperatures.

Conclusions

In this paper, a two-surface (TY coupled with MY) based elastoplastic constitutive model is developed in the critical state framework for describing the thermomechanical behaviour of saturated fine-grained soils. The TY and MY mechanisms are coupled through the volumetric plastic strain which is expressed in terms of both stress and temperature. To better characterize the isotropic thermal deformation of soil, a TY surface is introduced and a new expression for the thermoplastic strains is proposed and validated. Both the size and the shape of the MY surface are allowed to vary with temperature, which dependent on the combined hardening mechanism of the preconsolidation pressure and the thermal dependent spacing ratio, respectively. A nonlinear relationship between the spacing ratio and temperature changes is defined based on available experimental observations. The soil stress dilatancy is related to the spacing ratio as well, thus a non-

associated thermal dependent plastic potential is obtained, by which some observed temperature effects on the flow rule are well captured. The number of model parameters is kept to a minimum. All the parameters have a clear physical interpretation, and a detailed procedure for determining each of them is presented.

The model is evaluated by comparing with selected experimental results of several typical stress and temperature-controlled tests. It is demonstrated that many important thermomechanical features of saturated soils at non-isothermal conditions can be well described by the model, for example, thermal deformation of soil at different OCRs in one heating-cooling cycle, thermally induced overconsolidation effect observed in normally consolidated soils, and thermally induced soil strength changes (either increase or decrease) in both undrained and drained triaxial shear tests. It also reveals that further experimental and constitutive investigations, particularly, into the microscopic behaviour and mechanisms, are necessarily needed for better explaining and modelling some contrasting phenomena related to coupled thermal and mechanical effects.

Acknowledgement

The authors would like to acknowledge the National Natural Science Foundation of China (41502271), the State Key Laboratory for GeoMechanics and Deep Underground Engineering China University of Mining and Technology (SKLGDUEK1802), and the International Mobility Fund from the University of Leeds, which collectively supported this project. The second author also acknowledges the support of the ‘Taishan’ Scholar Program of Shandong Province, China (No. tsqn201909016) and the ‘Qilu’ Scholar Program of Shandong University.

References

Abuel-Naga, H., Bergado, D., Bouazza, A., and Ramana, G. 2007a. Volume change behaviour of saturated clays under drained heating conditions: experimental results and constitutive modeling. Canadian Geotechnical Journal, **44**(8): 942-956.

Abuel-Naga, H., Bergado, D., Bouazza, A., and Pender, M. 2009. Thermomechanical model for saturated clays. Geotechnique, **59**(3): 273-278.

Abuel-Naga, H.M., Bergado, D.T., and Lim, B.F. 2007b. Effect of temperature on shear strength and yielding behavior of soft Bangkok clay. Soils and Foundations, **47**(3): 423-436.

Atkinson, J. 2007. Peak strength of overconsolidated clays. Geotechnique, **57**(2): 127-135.

Baldi, G., Hueckel, T., and Pellegrini, R. 1988. Thermal volume changes of the mineral–water system in low-porosity clay soils. Canadian Geotechnical Journal, **25**(4): 807-825.

Baldi, G., Hueckel, T., Peano, A., and Pellegrini, R. 1991. Developments in modelling of thermohydro-geomechanical behaviour of Boom clay and clay-based buffer materials (Volume 1). EUR 13365/1, Commission of the European Communities, Luxembourg.

Barla, M., Di Donna, A., and Perino, A. 2016. Application of energy tunnels to an urban environment. Geothermics, **61**: 104-113.

Been, K., and Jefferies, M.G. 1985. A state parameter for sands. Geotechnique, **35**(2): 99-112.

Bourne-Webb, P., Burlon, S., Javed, S., Kürten, S., and Loveridge, F. 2016. Analysis and design methods for energy geostructures. Renewable and Sustainable Energy Reviews, **65**: 402-419.

Bourne-Webb, P., Amatya, B., Soga, K., Amis, T., Davidson, C., and Payne, P. 2009. Energy pile test at Lambeth College, London: geotechnical and thermodynamic aspects of pile response to heat cycles. Geotechnique, **59**(3): 237-248.

Burghignoli, A., Desideri, A., and Miliziano, S. 1992. Deformability of clays under non isothermal conditions. Rivista Italiana di Geotecnica, **92**(4): 227-236.

Campanella, R.G., and Mitchell, J.K. 1968. Influence of temperature variations on soil behavior. Journal of Soil Mechanics and Foundations Division, **94**: 709-734.

642 Cekerevac, C., and Laloui, L. 2004. Experimental study of thermal effects on the
643 mechanical behaviour of a clay. International Journal for Numerical and Analytical
644 Methods in Geomechanics, **28**(3): 209-228.
645 Chen, G., Chenevert, M.E., Sharma, M.M., and Yu, M. 2003. A study of wellbore stability
646 in shales including poroelastic, chemical, and thermal effects. Journal of Petroleum
647 Science and Engineering, **38**(3-4): 167-176.
648 Coccia, C.J.R., and McCartney, J.S. 2016. Thermal volume change of poorly draining
649 soils II: model development and experimental validation. Computers and
650 Geotechnics, **80**: 16-25.
651 Collins, I.F., and Kelly, P.A. 2002. A thermomechanical analysis of a family of soil
652 models. Geotechnique, **52**(7): 507-518.
653 Cui, Y.J., Sultan, N., and Delage, P. 2000. A thermomechanical model for saturated clays.
654 Canadian Geotechnical Journal, **37**(3): 607-620.
655 Dafalias, Y., and Taiebat, M. 2013. Anatomy of rotational hardening in clay plasticity.
656 Geotechnique, **63**(16): 1406-1418.
657 Dafalias, Y.F. 1986. Bounding surface plasticity. I: Mathematical foundation and
658 hypoplasticity. Journal of Engineering Mechanics, **112**(9): 966-987.
659 Demars, K., and Charles, R. 1982. Soil volume changes induced by temperature cycling.
660 Canadian Geotechnical Journal, **19**(2): 188-194.
661 Di Donna, A., Cecinato, F., Loveridge, F., and Barla, M. 2017. Energy performance of
662 diaphragm walls used as heat exchangers. Proceedings of the Institution of Civil
663 Engineers-Geotechnical Engineering, **170**(3): 232-245.
664 di Schio, E.R., Lazzari, S., and Abbati, A. 2016. Natural convection effects in the heat
665 transfer from a buried pipeline. Applied Thermal Engineering, **102**: 227-233.
666 Eriksson, L. 1989. Temperature effects on consolidation properties of sulphide clays. *In*
667 12th International Conference on Soil Mechanics and Foundation Engineering, Rio
668 de Janeiro. pp. 2087-2090.
669 Ghahremannejad, B. 2003. Thermo-mechanical behaviour of two reconstituted clays.
670 University of Sydney, Sydney, Australia.
671 Graham, J., Tanaka, N., Crilly, T., and Alfaro, M. 2001. Modified Cam-Clay modelling
672 of temperature effects in clays. Canadian Geotechnical Journal, **38**(3): 608-621.
673 Graham, J., Chandler, N.A., Dixon, D.A., Roach, P.J., To, T., and Wan, A.W.L. 1997.
674 The buffer/container experiment: results, synthesis, issues. Whiteshell Laboratories

675 Atonic Energy of Canada Limited Report AECL 11746 and CANDU Owners Group
676 Report COG-97-46-1, Pinawa, Manitoba.
677 Hamidi, A., and Khazaei, C. 2010. A thermo-mechanical constitutive model for saturated
678 clays. International Journal of Geotechnical Engineering, **4**(4): 445-459.
679 Hamidi, A., Tourchi, S., and Khazaei, C. 2014. Thermomechanical constitutive model for
680 saturated clays based on critical state theory. International Journal of Geomechanics,
681 **15**(1): 04014038.
682 Hardin, B.O., and Black, W.L. 1968. Vibration modulus of normally consolidated clay.
683 Journal of the Soil Mechanics and foundations Division, **94**(2): 353-370.
684 Hong, P., Pereira, J., Tang, A., and Cui, Y.-J. 2013. On some advanced thermo‐
685 mechanical models for saturated clays. International Journal for Numerical and
686 Analytical Methods in Geomechanics, **37**(17): 2952-2971.
687 Hong, P.Y., Pereira, J.-M., Cui, Y.J., and Tang, A.M. 2016. A two‐surface
688 thermomechanical model for saturated clays. International Journal for Numerical and
689 Analytical Methods in Geomechanics, **40**(7): 1059-1080.
690 Hueckel, T., and Borsetto, M. 1990. Thermoplasticity of saturated soils and shales:
691 constitutive equations. Journal of geotechnical engineering, **116**(12): 1765-1777.
692 Hueckel, T., and Baldi, G. 1990. Thermoplasticity of saturated clays: experimental
693 constitutive study. Journal of geotechnical engineering, **116**(12): 1778-1796.
694 Hueckel, T., and Pellegrini, R. 1991. Thermoplastic modeling of undrained failure of
695 saturated clay due to heating. Soils and Foundations, **31**(3): 1-16.
696 Hueckel, T., François, B., and Laloui, L. 2009. Explaining thermal failure in saturated
697 clays. Geotechnique, **59**(3): 197-212.
698 Jin, Y.-F., Wu, Z.-X., Yin, Z.-Y., and Shen, J.S. 2017. Estimation of critical state-related
699 formula in advanced constitutive modeling of granular material. Acta Geotechnica,
700 **12**(6): 1329-1351.
701 Khalili, N., Uchaipichat, A., and Javadi, A. 2010. Skeletal thermal expansion coefficient
702 and thermo-hydro-mechanical constitutive relations for saturated homogeneous
703 porous media. Mechanics of Materials, **42**(6): 593-598.
704 Kuntiwattanakul, P., Towhata, I., Ohishi, K., and Seko, I. 1995. Temperature effects on
705 undrained shear characteristics of clay. Soils and Foundations, **35**(1): 147-162.
706 Laloui, L., and Cekerevac, C. 2003. Thermo-plasticity of clays: an isotropic yield
707 mechanism. Computers and Geotechnics, **30**(8): 649-660.

708 Laloui, L., and François, B. 2009. ACMEG-T: soil thermoplasticity model. Journal of
709 Engineering Mechanics, **135**(9): 932-944.
710 Laloui, L., and Di Donna, A. 2013. Energy geostructures: innovation in underground
711 engineering. John Wiley & Sons.
712 Laloui, L., Nuth, M., and Vulliet, L. 2006. Experimental and numerical investigations of
713 the behaviour of a heat exchanger pile. International Journal for Numerical and
714 Analytical Methods in Geomechanics, **30**(8): 763-781.
715 Lingnau, B., Graham, J., and Tanaka, N. 1995. Isothermal modeling of sand–bentonite
716 mixtures at elevated temperatures. Canadian Geotechnical Journal, **32**(1): 78-88.
717 Liu, E.L., and Xing, H.L. 2009. A double hardening thermo-mechanical constitutive
718 model for overconsolidated clays. Acta Geotechnica, **4**(1): 1-6.
719 Mašín, D., and Khalili, N. 2012. A thermo‐mechanical model for variably saturated
720 soils based on hypoplasticity. International Journal for Numerical and Analytical
721 Methods in Geomechanics, **36**(12): 1461-1485.
722 Mattsson, H., Axelsson, K., and Klisinski, M. 1999. On a constitutive driver as a useful
723 tool in soil plasticity. Advances in Engineering Software, **30**(8): 511-528.
724 McDowell, G.R., and Hau, K.W. 2003. A simple non-associated three surface kinematic
725 hardening model. Geotechnique, **53**(4): 433-437.
726 Mita, K.A., Dasari, G.R., and Lo, K.W. 2004. Performance of a three-dimensional
727 Hvorslev–modified Cam clay model for overconsolidated clay. International Journal
728 of Geomechanics, **4**(4): 296-309.
729 Mitchell, J.K., and Abdel-hadi, O.N. 1979. Temperature distributions around buried
730 cables. IEEE Transactions on Power Apparatus and Systems, **PAS-98**(4): 1158-1166.
731 Moritz, L. 1995. Geotechnical properties of clay at elevated temperatures. Swedish
732 Geotechnical Institute Linköping, Sweden.
733 Naylor, D.J. 1985. A continuous plasticity version of the critical state model. International
734 Journal for Numerical Methods in Engineering, **21**(7): 1187-1204.
735 Pinyol, N., Alvarado, M., Alonso, E., and Zabala, F. 2017. Thermal effects in landslide
736 mobility. Geotechnique, **68**(6): 528-545.
737 Plum, R.L., and Esrig, M.I. 1969. Some temperature effects on soil compressibility and
738 pore water pressure. Highway Research Board Special Report 103, Highway
739 Research Board, Washington, D.C.

740 Robinet, J.-C., Rahbaoui, A., Plas, F., and Lebon, P. 1996. A constitutive
741 thermomechanical model for saturated clays. Engineering Geology, **41**(1-4): 145-169.
742 Roscoe, K.H., and Burland, J.B. 1968. On the generalized stress-strain behaviour of wet
743 clay. *In* Engineering Plasticity. *Edited by* G. Heymann and F.A. Leckie. Cambridge
744 University Press, London, UK. pp. 535-609.
745 Roscoe, K.H., Schofield, A.N., and Wroth, C.P. 1958. On the yielding of soils.
746 Geotechnique, **8**(1): 22-53.
747 Schofield, A.N., and Wroth, C.P. 1968. Critical state soil mechanics. McGraw-Hill,
748 London.
749 Seneviratne, H., Carter, J., Airey, D., and Booker, J. 1993. A review of models for
750 predicting the thermomechanical behaviour of soft clays. International Journal for
751 Numerical and Analytical Methods in Geomechanics, **17**(10): 715-733.
752 Sultan, N., Delage, P., and Cui, Y. 2002. Temperature effects on the volume change
753 behaviour of Boom clay. Engineering Geology, **64**(2): 135-145.
754 Tanaka, N. 1995. Thermal elastic plastic behaviour and modelling of saturated clays.
755 University of Manitoba, Hinnipeg, Manitoba, Canada.
756 Tanaka, N., Graham, J., and Crilly, T. 1997. Stress-strain behaviour of reconstituted illitic
757 clay at different temperatures. Engineering Geology, **47**(4): 339-350.
758 Teltayev, B., and Suppes, E. 2019. Temperature in pavement and subgrade and its effect
759 on moisture. Case Studies in Thermal Engineering, **13**: 100363.
760 Towhata, I., Kuntiwattanaku, P., Seko, I., and Ohishi, K. 1993. Volume change of clays
761 induced by heating as observed in consolidation tests. Soils and Foundations, **33**(4):
762 170-183.
763 Uchaipichat, A., and Khalili, N. 2009. Experimental investigation of thermo-hydro-
764 mechanical behaviour of an unsaturated silt. Geotechnique, **59**(4): 339-353.
765 Vardanega, P., and Bolton, M. 2013. Stiffness of clays and silts: Normalizing shear
766 modulus and shear strain. Journal of Geotechnical and Geoenvironmental
767 Engineering, **139**(9): 1575-1589.
768 Wang, L., Wang, K., and Hong, Y. 2016. Modeling temperature-dependent behavior of
769 soft clay. Journal of Engineering Mechanics, **142**(8): 04016054.
770 Wheeler, S.J., Näätänen, A., Karstunen, M., and Lojander, M. 2003. An anisotropic
771 elastoplastic model for soft clays. Canadian Geotechnical Journal, **40**(2): 403-418.
772 Wood, D.M. 1990. Soil behaviour and critical state soil mechanics. Cambridge University
773 Press, Cambridge, UK.

774 Wroth, C.P. 1984. The interpretation of in situ soil tests. Geotechnique, **34**(4): 449-489.
775 Yao, Y.P., and Zhou, A.N. 2013. Non-isothermal unified hardening model: a thermo-
776 elasto-plastic model for clays. Geotechnique, **63**(15): 1328.
777 Yao, Y.P., Hou, W., and Zhou, A.N. 2009. UH model: three-dimensional unified
778 hardening model for overconsolidated clays. Geotechnique, **59**(5): 451-469.
779 Yin, Z.-Y., Jin, Y.-F., Shen, S.-L., and Huang, H.-W. 2017. An efficient optimization
780 method for identifying parameters of soft structured clay by an enhanced genetic
781 algorithm and elastic–viscoplastic model. Acta Geotechnica, **12**(4): 849-867.
782 Yin, Z.Y., Jin, Y.F., Shen, J.S., and Hicher, P.Y. 2018. Optimization techniques for
783 identifying soil parameters in geotechnical engineering: Comparative study and
784 enhancement. International Journal for Numerical and Analytical Methods in
785 Geomechanics, **42**(1): 70-94.
786 Yu, H.S. 1998. CASM: A unified state parameter model for clay and sand. International
787 Journal for Numerical and Analytical Methods in Geomechanics, **22**(8): 621-653.
788 Yu, H.S. 2006. Plasticity and geotechnics. Springer Science & Business Media, New
789 York, USA.
790 Yu, H.S., Khong, C.D., Wang, J., and Zhang, G. 2005. Experimental evaluation and
791 extension of a simple critical state model for sand. Granular Matter, **7**(4): 213-225.
792 Zhou, C., and Ng, C.W.W. 2015. A thermomechanical model for saturated soil at small
793 and large strains. Canadian Geotechnical Journal, **52**(8): 1101-1110.

Table and Figure captions

Notation

p, q	effective mean and deviatoric stress
e	void ratio
v	soil specific volume, v=1+e
T_0	room temperature
$p_{c(\mathrm{T})}$	preconsolidation pressure at temperature T
$p_{\mathrm{c0}(\mathrm{T}_0)}$	initial preconsolidation pressure at T_0
$p_{x(\mathrm{T})}$	critical state stress at temperature T
f^{MY}, f^{TY}	mechanical and thermal yield limits
$r_{(\mathrm{T})}$	spacing rato at temperature T, $r_{(\mathrm{T})} = p_{c(\mathrm{T})} / p_{x(\mathrm{T})}$
η	stress ratio, $\eta = q / p$
M	the slope of the CSL in the p - q space
n	stress state coefficient
$\xi_{(\mathrm{T})}$	state parameter at temperature T
$\xi_{R(\mathrm{T})}$	vertical distance between the NCL and the CSL
$N_{(\mathrm{T})}$	specific volume on the NCL at $p = 1\mathrm{kPa}$ at temperature T
$\Gamma_{(\mathrm{T})}$	specific volume on CSL at $p = 1\mathrm{kPa}$ at temperature T
λ	the slope of the NCL in the v-ln p space
κ	the slope of the swelling line in the v-ln p space
$p_{\mathrm{T}(\mathrm{T})}$	effective stress at the transition temperature
$\varepsilon_{\mathrm{v}}^{\mathrm{e}}$, $\varepsilon_{\mathrm{d}}^{\mathrm{e}}$	elastic volumetric strain and elastic deviatoric strain
$\varepsilon_{\mathrm{v}}^{p}$, $\varepsilon_{\mathrm{d}}^{p}$	plastic volumetric strain and elastic deviatoric strain
μ	Poisson's ratio
α	drained elastic volumetric thermal expansion coefficient
$\varepsilon_{v}^{\mathrm{mp}}$, $\varepsilon_{\mathrm{v}}^{\mathrm{tp}}$	mechanical and thermal components of $\varepsilon_{\mathrm{v}}^{p}$
$\varepsilon_{\mathrm{d}}^{\mathrm{mp}}$	mechanical component of $\varepsilon_{\mathrm{v}}^{p}$
g^{MY}	mechanical plastic potential
$\mathrm{d}\lambda_{\mathrm{m}}$	is the plastic multiplier
θ	material parameter for thermal evolution of the preconsolidation pressure

ζ	material parameter for thermal evolution of the spacing ratio
β (or β_0)	material parameter for thermal evolution of TY
ω	material parameter controlling the development of ε_v^{tp}

Abuel-Naga, H., Bergado, D., Bouazza, A., and Ramana, G. 2007a. Volume change behaviour of saturated clays under drained heating conditions: experimental results and constitutive modeling. Canadian Geotechnical Journal, **44**(8): 942-956.

Abuel-Naga, H., Bergado, D., Bouazza, A., and Pender, M. 2009. Thermomechanical model for saturated clays. Geotechnique, **59**(3): 273-278.

Abuel-Naga, H.M., Bergado, D.T., and Lim, B.F. 2007b. Effect of temperature on shear strength and yielding behavior of soft Bangkok clay. Soils and Foundations, **47**(3): 423-436.

Bai, B., Yang, G.-c., Li, T., and Yang, G.-s. 2019. A thermodynamic constitutive model with temperature effect based on particle rearrangement for geomaterials. Mechanics of Materials, **139**: 103180.

Baldi, G., Hueckel, T., and Pellegrini, R. 1988. Thermal volume changes of the mineral–water system in low-porosity clay soils. Canadian Geotechnical Journal, **25**(4): 807-825.

Baldi, G., Hueckel, T., Peano, A., and Pellegrini, R. 1991. Developments in modelling of thermohydro-geomechanical behaviour of Boom clay and clay-based buffer materials (Volume 1). EUR 13365/1, Commission of the European Communities, Luxembourg.

Barla, M., Di Donna, A., and Perino, A. 2016. Application of energy tunnels to an urban environment. Geothermics, **61**: 104-113.

Been, K., and Jefferies, M.G. 1985. A state parameter for sands. Geotechnique, **35**(2): 99-112.

Bourne-Webb, P., Freitas, T.B., and Assunção, R.F. 2019. A review of pile-soil interactions in isolated, thermally-activated piles. Computers and Geotechnics, **108**: 61-74.

Bourne-Webb, P., Burlon, S., Javed, S., Kürten, S., and Loveridge, F. 2016. Analysis and design methods for energy geostructures. Renewable and Sustainable Energy Reviews, **65**: 402-419.

881 Burghignoli, A., Desideri, A., and Miliziano, S. 1992. Deformability of clays under non
882 isothermal conditions. Rivista Italiana di Geotecnica, **92**(4): 227-236.
883 Campanella, R.G., and Mitchell, J.K. 1968. Influence of temperature variations on soil
884 behavior. Journal of Soil Mechanics and Foundations Division, **94**: 709-734.
885 Cekerevac, C., and Laloui, L. 2004. Experimental study of thermal effects on the
886 mechanical behaviour of a clay. International Journal for Numerical and Analytical
887 Methods in Geomechanics, **28**(3): 209-228.
888 Chen, G., Chenevert, M.E., Sharma, M.M., and Yu, M. 2003. A study of wellbore stability
889 in shales including poroelastic, chemical, and thermal effects. Journal of Petroleum
890 Science and Engineering, **38**(3-4): 167-176.
891 Coccia, C.J.R., and McCartney, J.S. 2016. Thermal volume change of poorly draining
892 soils II: model development and experimental validation. Computers and
893 Geotechnics, **80**: 16-25.
894 Collins, I.F., and Kelly, P.A. 2002. A thermomechanical analysis of a family of soil
895 models. Geotechnique, **52**(7): 507-518.
896 Cui, Y.J., Sultan, N., and Delage, P. 2000. A thermomechanical model for saturated clays.
897 Canadian Geotechnical Journal, **37**(3): 607-620.
898 Dafalias, Y., and Taiebat, M. 2013. Anatomy of rotational hardening in clay plasticity.
899 Geotechnique, **63**(16): 1406-1418.
900 Dafalias, Y.F. 1986. Bounding surface plasticity. I: Mathematical foundation and
901 hypoplasticity. Journal of Engineering Mechanics, **112**(9): 966-987.
902 De Bruyn, D., and Thimus, J.-F. 1996. The influence of temperature on mechanical
903 characteristics of Boom clay: the results of an initial laboratory programme.
904 Engineering Geology, **41**(1-4): 117-126.
905 Demars, K., and Charles, R. 1982. Soil volume changes induced by temperature cycling.
906 Canadian Geotechnical Journal, **19**(2): 188-194.
907 Di Donna, A., and Laloui, L. 2015. Response of soil subjected to thermal cyclic loading:
908 experimental and constitutive study. Engineering Geology, **190**: 65-76.
909 Di Donna, A., Cecinato, F., Loveridge, F., and Barla, M. 2017. Energy performance of
910 diaphragm walls used as heat exchangers. Proceedings of the Institution of Civil
911 Engineers-Geotechnical Engineering, **170**(3): 232-245.
912 di Schio, E.R., Lazzari, S., and Abbati, A. 2016. Natural convection effects in the heat
913 transfer from a buried pipeline. Applied Thermal Engineering, **102**: 227-233.

914 Eriksson, L. 1989. Temperature effects on consolidation properties of sulphide clays. *In*
915 12th International Conference on Soil Mechanics and Foundation Engineering, Rio
916 de Janeiro. pp. 2087-2090.
917 Ghahremannejad, B. 2003. Thermo-mechanical behaviour of two reconstituted clays.
918 University of Sydney, Sydney, Australia.
919 Graham, J., Tanaka, N., Crilly, T., and Alfaro, M. 2001. Modified Cam-Clay modelling
920 of temperature effects in clays. Canadian Geotechnical Journal, **38**(3): 608-621.
921 Graham, J., Chandler, N.A., Dixon, D.A., Roach, P.J., To, T., and Wan, A.W.L. 1997.
922 The buffer/container experiment: results, synthesis, issues. Whiteshell Laboratories
923 Atonic Energy of Canada Limited Report AECL 11746 and CANDU Owners Group
924 Report COG-97-46-1, Pinawa, Manitoba.
925 Hamidi, A., and Khazaei, C. 2010. A thermo-mechanical constitutive model for saturated
926 clays. International Journal of Geotechnical Engineering, **4**(4): 445-459.
927 Hamidi, A., Tourchi, S., and Khazaei, C. 2015. Thermomechanical constitutive model for
928 saturated clays based on critical state theory. International Journal of Geomechanics,
929 **15**(1): 04014038.
930 Hardin, B.O., and Black, W.L. 1968. Vibration modulus of normally consolidated clay.
931 Journal of the Soil Mechanics and foundations Division, **94**(2): 353-370.
932 Hong, P., Pereira, J., Tang, A., and Cui, Y.-J. 2013. On some advanced thermo‐
933 mechanical models for saturated clays. International Journal for Numerical and
934 Analytical Methods in Geomechanics, **37**(17): 2952-2971.
935 Hong, P.Y., Pereira, J.-M., Cui, Y.J., and Tang, A.M. 2016. A two‐surface
936 thermomechanical model for saturated clays. International Journal for Numerical and
937 Analytical Methods in Geomechanics, **40**(7): 1059-1080.
938 Hueckel, T., and Borsetto, M. 1990. Thermoplasticity of saturated soils and shales:
939 constitutive equations. Journal of geotechnical engineering, **116**(12): 1765-1777.
940 Hueckel, T., and Baldi, G. 1990. Thermoplasticity of saturated clays: experimental
941 constitutive study. Journal of geotechnical engineering, **116**(12): 1778-1796.
942 Hueckel, T., and Pellegrini, R. 1991. Thermoplastic modeling of undrained failure of
943 saturated clay due to heating. Soils and Foundations, **31**(3): 1-16.
944 Hueckel, T., François, B., and Laloui, L. 2009. Explaining thermal failure in saturated
945 clays. Geotechnique, **59**(3): 197-212.

946 Jin, Y.-F., Wu, Z.-X., Yin, Z.-Y., and Shen, J.S. 2017. Estimation of critical state-related
947 formula in advanced constitutive modeling of granular material. Acta Geotechnica,
948 **12**(6): 1329-1351.
949 Khalili, N., Uchaipichat, A., and Javadi, A. 2010. Skeletal thermal expansion coefficient
950 and thermo-hydro-mechanical constitutive relations for saturated homogeneous
951 porous media. Mechanics of Materials, **42**(6): 593-598.
952 Kuntiwattanakul, P., Towhata, I., Ohishi, K., and Seko, I. 1995. Temperature effects on
953 undrained shear characteristics of clay. Soils and Foundations, **35**(1): 147-162.
954 Laloui, L., and Cekerevac, C. 2003. Thermo-plasticity of clays: an isotropic yield
955 mechanism. Computers and Geotechnics, **30**(8): 649-660.
956 Laloui, L., and François, B. 2009. ACMEG-T: soil thermoplasticity model. Journal of
957 Engineering Mechanics, **135**(9): 932-944.
958 Laloui, L., and Di Donna, A. 2013. Energy geostructures: innovation in underground
959 engineering. John Wiley & Sons.
960 Laloui, L., Nuth, M., and Vulliet, L. 2006. Experimental and numerical investigations of
961 the behaviour of a heat exchanger pile. International Journal for Numerical and
962 Analytical Methods in Geomechanics, **30**(8): 763-781.
963 Li, X., Feng, Y., El Mohtar, C.S., and Gray, K. 2019. Transient modeling of borehole
964 breakouts: A coupled thermo-hydro-mechanical approach. Journal of Petroleum
965 Science and Engineering, **172**: 1014-1024.
966 Lingnau, B., Graham, J., and Tanaka, N. 1995. Isothermal modeling of sand–bentonite
967 mixtures at elevated temperatures. Canadian Geotechnical Journal, **32**(1): 78-88.
968 Liu, E.L., and Xing, H.L. 2009. A double hardening thermo-mechanical constitutive
969 model for overconsolidated clays. Acta Geotechnica, **4**(1): 1-6.
970 Mašín, D., and Khalili, N. 2012. A thermo‐mechanical model for variably saturated
971 soils based on hypoplasticity. International Journal for Numerical and Analytical
972 Methods in Geomechanics, **36**(12): 1461-1485.
973 Mattsson, H., Axelsson, K., and Klisinski, M. 1999. On a constitutive driver as a useful
974 tool in soil plasticity. Advances in Engineering Software, **30**(8): 511-528.
975 McDowell, G.R., and Hau, K.W. 2003. A simple non-associated three surface kinematic
976 hardening model. Geotechnique, **53**(4): 433-437.
977 Mitchell, J.K., and Abdel-hadi, O.N. 1979. Temperature distributions around buried
978 cables. IEEE transactions on power apparatus and systems, **PAS-98**(4): 1158-1166.

Moritz, L. 1995. Geotechnical properties of clay at elevated temperatures. Swedish Geotechnical Institute Linköping, Sweden.

Ng, C.W.W., Mu, Q., and Zhou, C. 2018. Effects of specimen preparation method on the volume change of clay under cyclic thermal loads. Geotechnique: 1-5.

Pinyol, N., Alvarado, M., Alonso, E., and Zabala, F. 2017. Thermal effects in landslide mobility. Geotechnique, **68**(6): 528-545.

Plum, R.L., and Esrig, M.I. 1969. Some temperature effects on soil compressibility and pore water pressure. Highway Research Board Special Report 103, Highway Research Board, Washington, D.C.

Robinet, J.-C., Rahbaoui, A., Plas, F., and Lebon, P. 1996. A constitutive thermomechanical model for saturated clays. Engineering Geology, **41**(1-4): 145-169.

Roscoe, K.H., and Burland, J.B. 1968. On the generalized stress-strain behaviour of wet clay. *In* Engineering Plasticity. *Edited by* G. Heymann and F.A. Leckie. Cambridge University Press, London, UK. pp. 535-609.

Roscoe, K.H., Schofield, A.N., and Wroth, C.P. 1958. On the yielding of soils. Geotechnique, **8**(1): 22-53.

Schofield, A.N., and Wroth, C.P. 1968. Critical state soil mechanics. McGraw-Hill, London.

Seneviratne, H., Carter, J., Airey, D., and Booker, J. 1993. A review of models for predicting the thermomechanical behaviour of soft clays. International Journal for Numerical and Analytical Methods in Geomechanics, **17**(10): 715-733.

Shetty, R., Singh, D., and Ferrari, A. 2019. Volume change characteristics of fine-grained soils due to sequential thermo-mechanical stresses. Engineering Geology, **253**: 47-54.

Sultan, N., Delage, P., and Cui, Y. 2002. Temperature effects on the volume change behaviour of Boom clay. Engineering Geology, **64**(2): 135-145.

Tanaka, N. 1995. Thermal elastic plastic behaviour and modelling of saturated clays. University of Manitoba, Hinnipeg, Manitoba, Canada.

Tanaka, N., Graham, J., and Crilly, T. 1997. Stress-strain behaviour of reconstituted illitic clay at different temperatures. Engineering Geology, **47**(4): 339-350.

Teltayev, B., and Suppes, E. 2019. Temperature in pavement and subgrade and its effect on moisture. Case Studies in Thermal Engineering, **13**: 100363.

Towhata, I., Kuntiwattanaku, P., Seko, I., and Ohishi, K. 1993. Volume change of clays induced by heating as observed in consolidation tests. Soils and Foundations, **33**(4): 170-183.

1013 Uchaipichat, A., and Khalili, N. 2009. Experimental investigation of thermo-hydro-
1014 mechanical behaviour of an unsaturated silt. Geotechnique, **59**(4): 339-353.
1015 Vardanega, P., and Bolton, M. 2013. Stiffness of clays and silts: Normalizing shear
1016 modulus and shear strain. Journal of Geotechnical and Geoenvironmental
1017 Engineering, **139**(9): 1575-1589.
1018 Wang, L., Wang, K., and Hong, Y. 2016. Modeling temperature-dependent behavior of
1019 soft clay. Journal of Engineering Mechanics, **142**(8): 04016054.
1020 Wheeler, S.J., Näätänen, A., Karstunen, M., and Lojander, M. 2003. An anisotropic
1021 elastoplastic model for soft clays. Canadian Geotechnical Journal, **40**(2): 403-418.
1022 Wood, D.M. 1990. Soil behaviour and critical state soil mechanics. Cambridge University
1023 Press, Cambridge, UK.
1024 Wroth, C.P. 1984. The interpretation of in situ soil tests. Geotechnique, **34**(4): 449-489.
1025 Xiao, H. 2014. Thermo-coupled elastoplasticity models with asymptotic loss of the
1026 material strength. International Journal of Plasticity, **63**: 211-228.
1027 Yao, Y.P., and Zhou, A.N. 2013. Non-isothermal unified hardening model: a thermo-
1028 elasto-plastic model for clays. Geotechnique, **63**(15): 1328.
1029 Yin, Z.-Y., Jin, Y.-F., Shen, S.-L., and Huang, H.-W. 2017. An efficient optimization
1030 method for identifying parameters of soft structured clay by an enhanced genetic
1031 algorithm and elastic–viscoplastic model. Acta Geotechnica, **12**(4): 849-867.
1032 Yin, Z.Y., Jin, Y.F., Shen, J.S., and Hicher, P.Y. 2018. Optimization techniques for
1033 identifying soil parameters in geotechnical engineering: Comparative study and
1034 enhancement. International Journal for Numerical and Analytical Methods in
1035 Geomechanics, **42**(1): 70-94.
1036 Yu, H.S. 1998. CASM: A unified state parameter model for clay and sand. International
1037 Journal for Numerical and Analytical Methods in Geomechanics, **22**(8): 621-653.
1038 Yu, H.S. 2006. Plasticity and geotechnics. Springer Science & Business Media, New
1039 York, USA.
1040 Yu, H.S., Khong, C.D., Wang, J., and Zhang, G. 2005. Experimental evaluation and
1041 extension of a simple critical state model for sand. Granular Matter, **7**(4): 213-225.
1042 Zhang, Z., and Cheng, X. 2017. A fully coupled THM model based on a non‐
1043 equilibrium thermodynamic approach and its application. International Journal for
1044 Numerical and Analytical Methods in Geomechanics, **41**(4): 527-554.

1045 Zhou, C., and Ng, C.W.W. 2015. A thermomechanical model for saturated soil at small
1046 and large strains. Canadian Geotechnical Journal, **52**(8): 1101-1110.
1047 Zymnis, D.M., Whittle, A.J., and Germaine, J.T. 2018. Measurement of Temperature-
1048 Dependent Bound Water in Clays. Geotechnical Testing Journal, **42**(1): 232-244.

1049

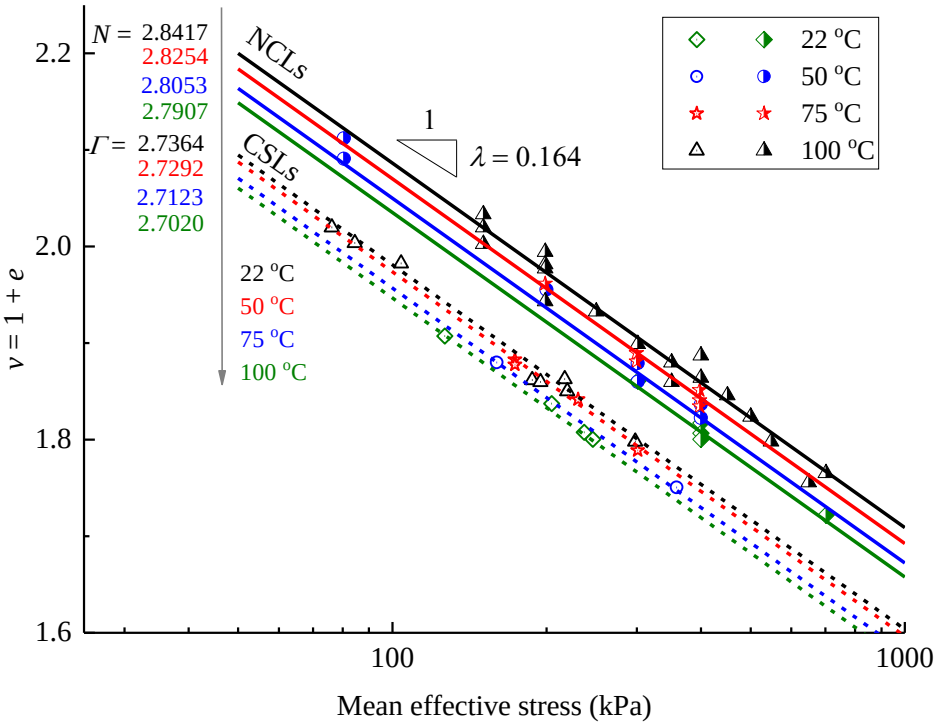

Fig. 1 Measured and fitted NCLs and CSLs for M44 clay at different temperatures (after Ghahremannejad (2003)).

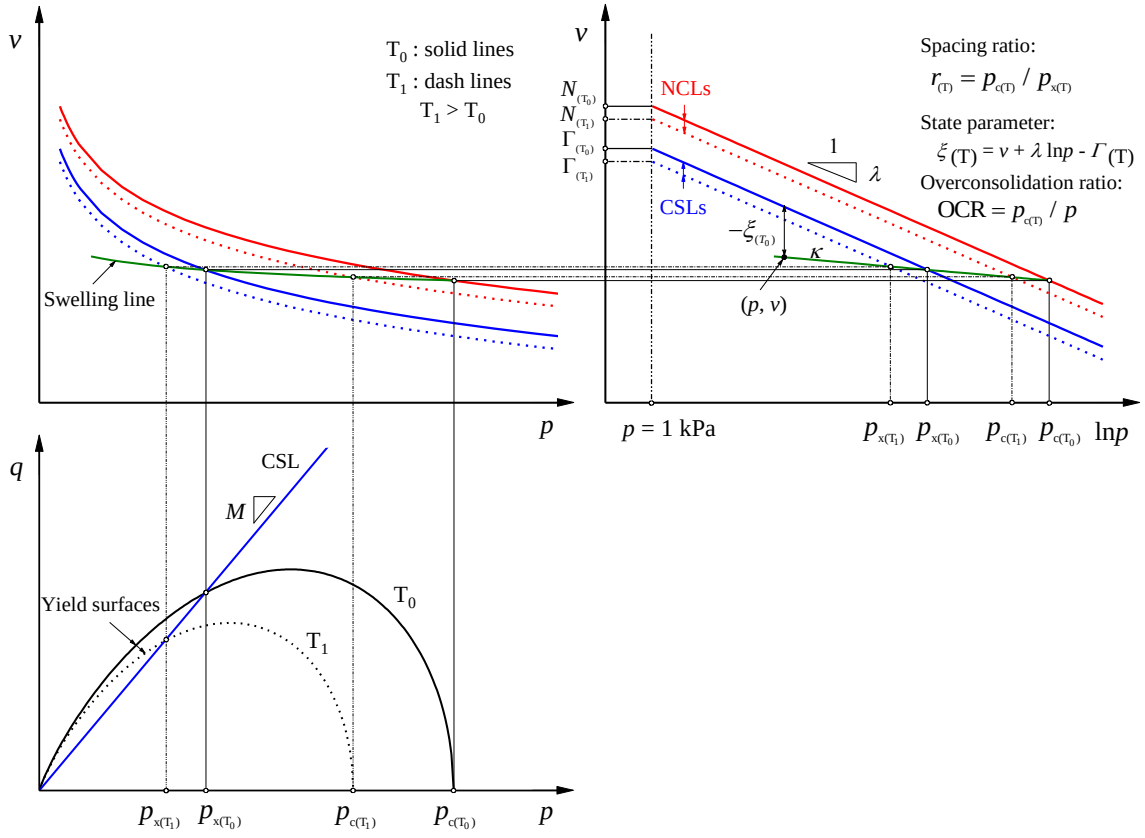

Fig. 2 Definitions and example relationships among NCLs, NCLs and yield loci.

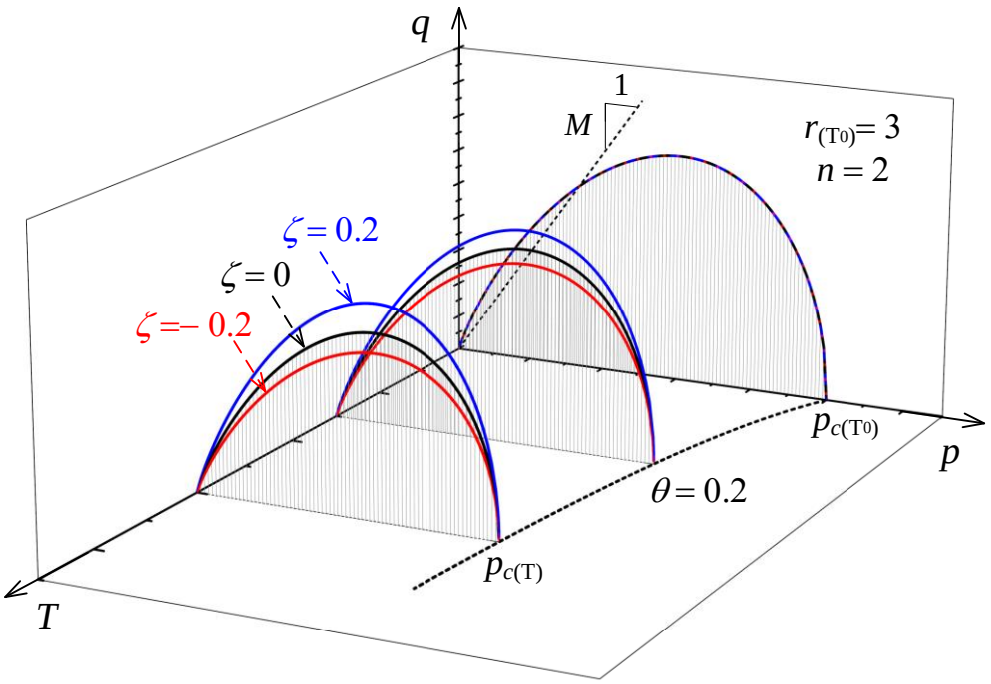

Fig. 3 Size and shape variation with temperature increase at constant plastic strain.

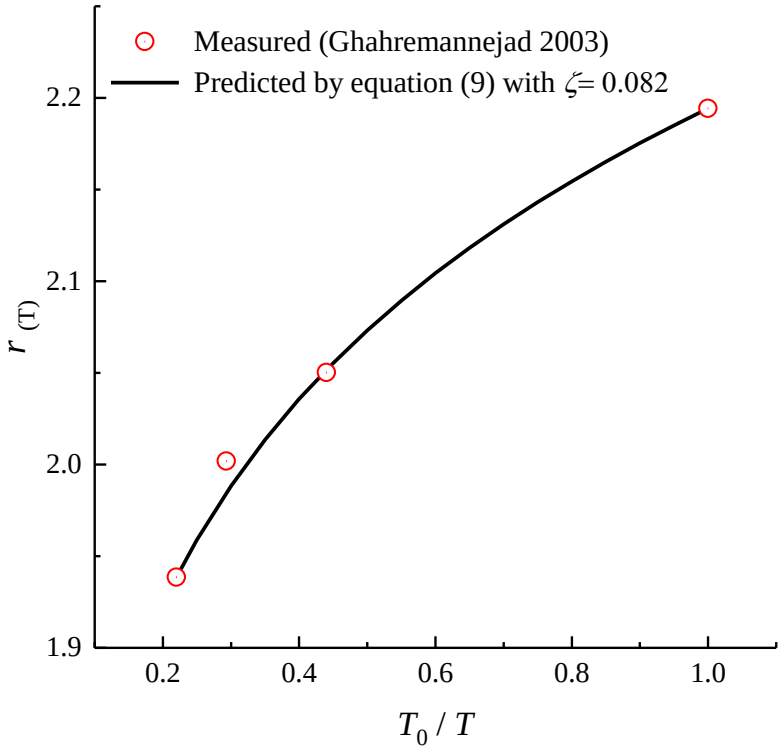

Fig. 4 Measured and predicted thermal variation of the spacing ratio for M44 clay.

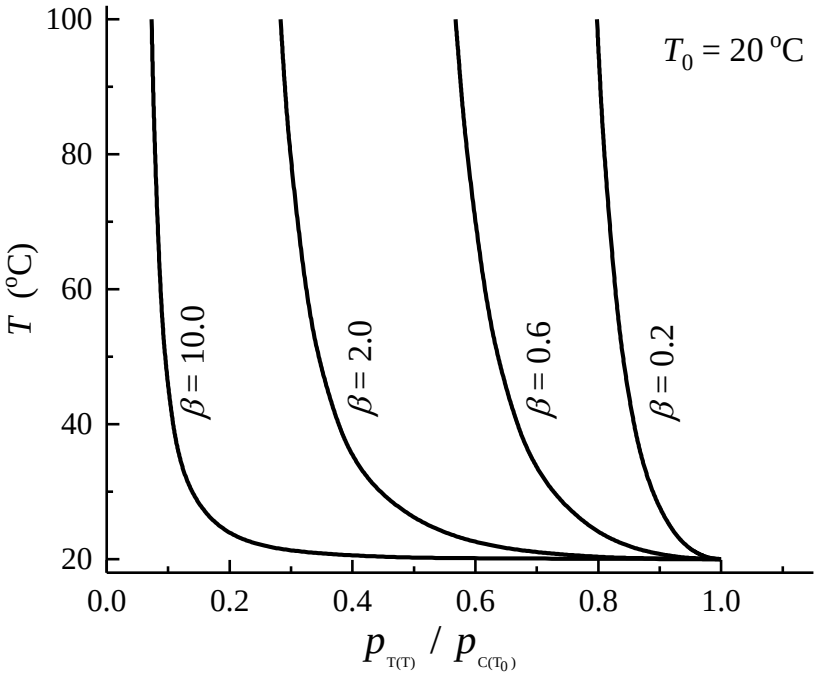

Fig. 5 Example results of TY limits.

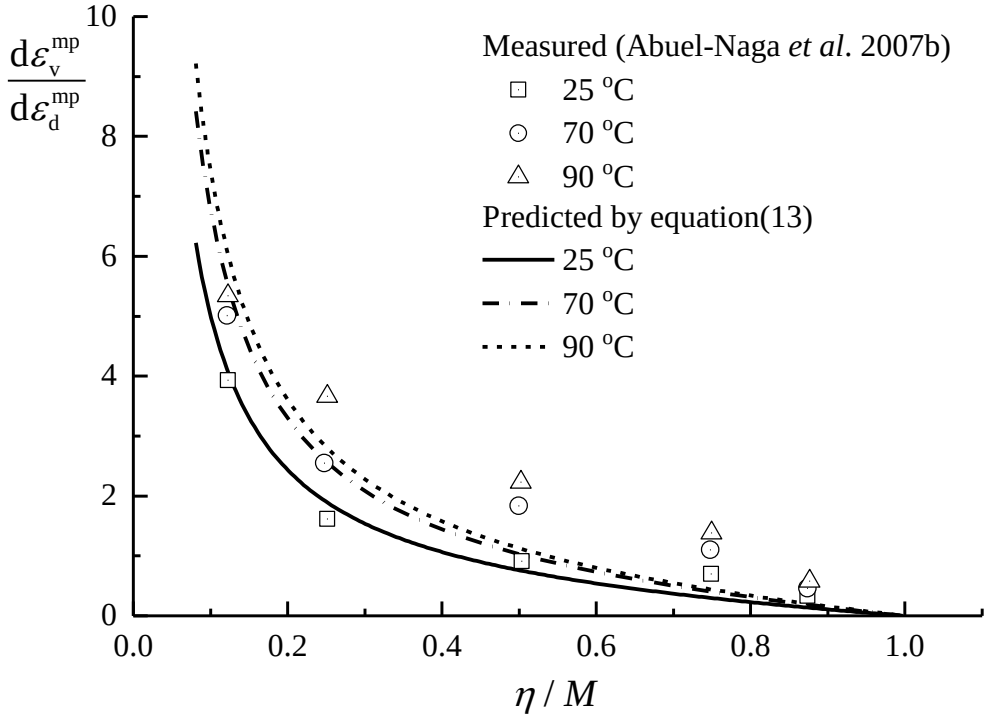

Fig. 6 Measured and predicted stress–dilatancy relationships for soft Bangkok clay.

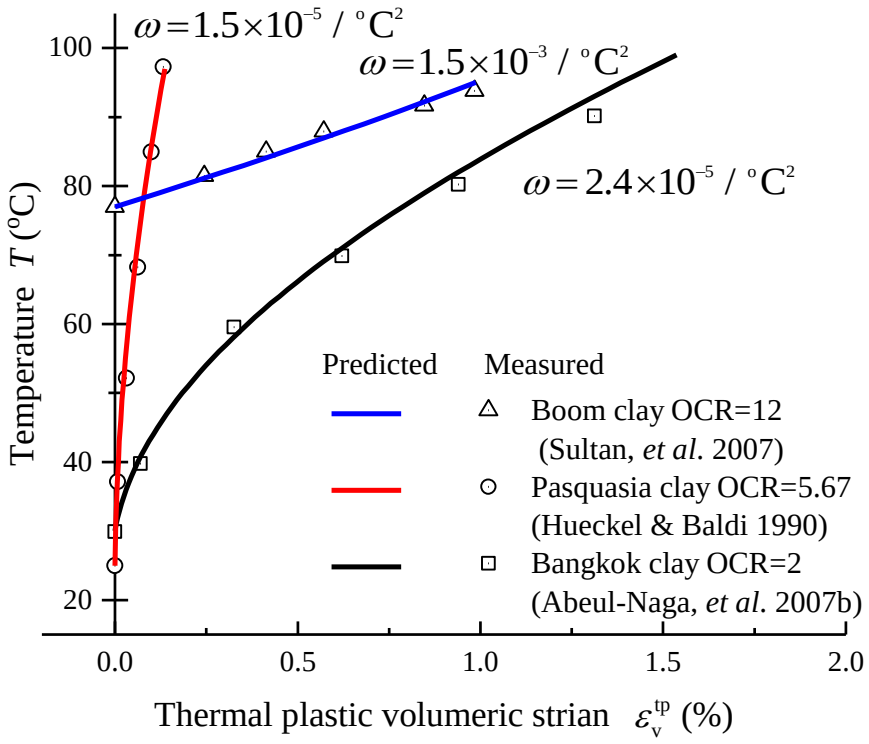

Fig. 7 Measured and predicted thermal plastic volumetric strains.

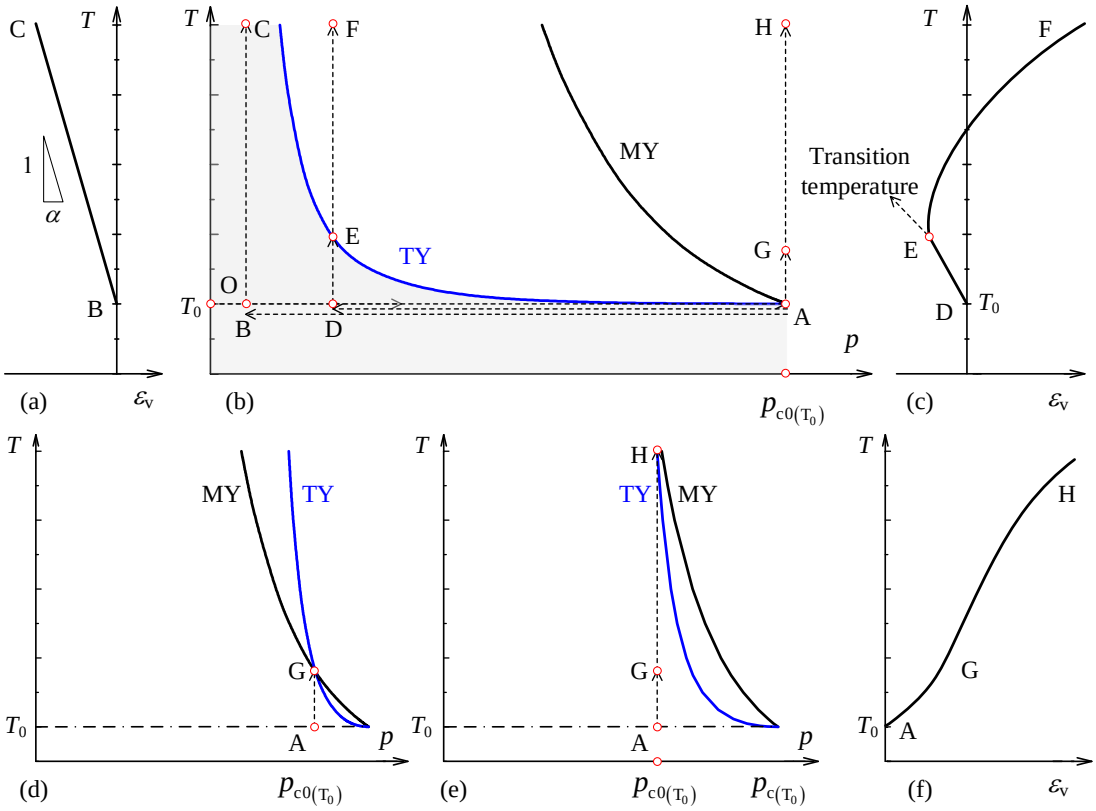

Fig. 8Explanation of model responses subjected to heating at three typical OCR values.

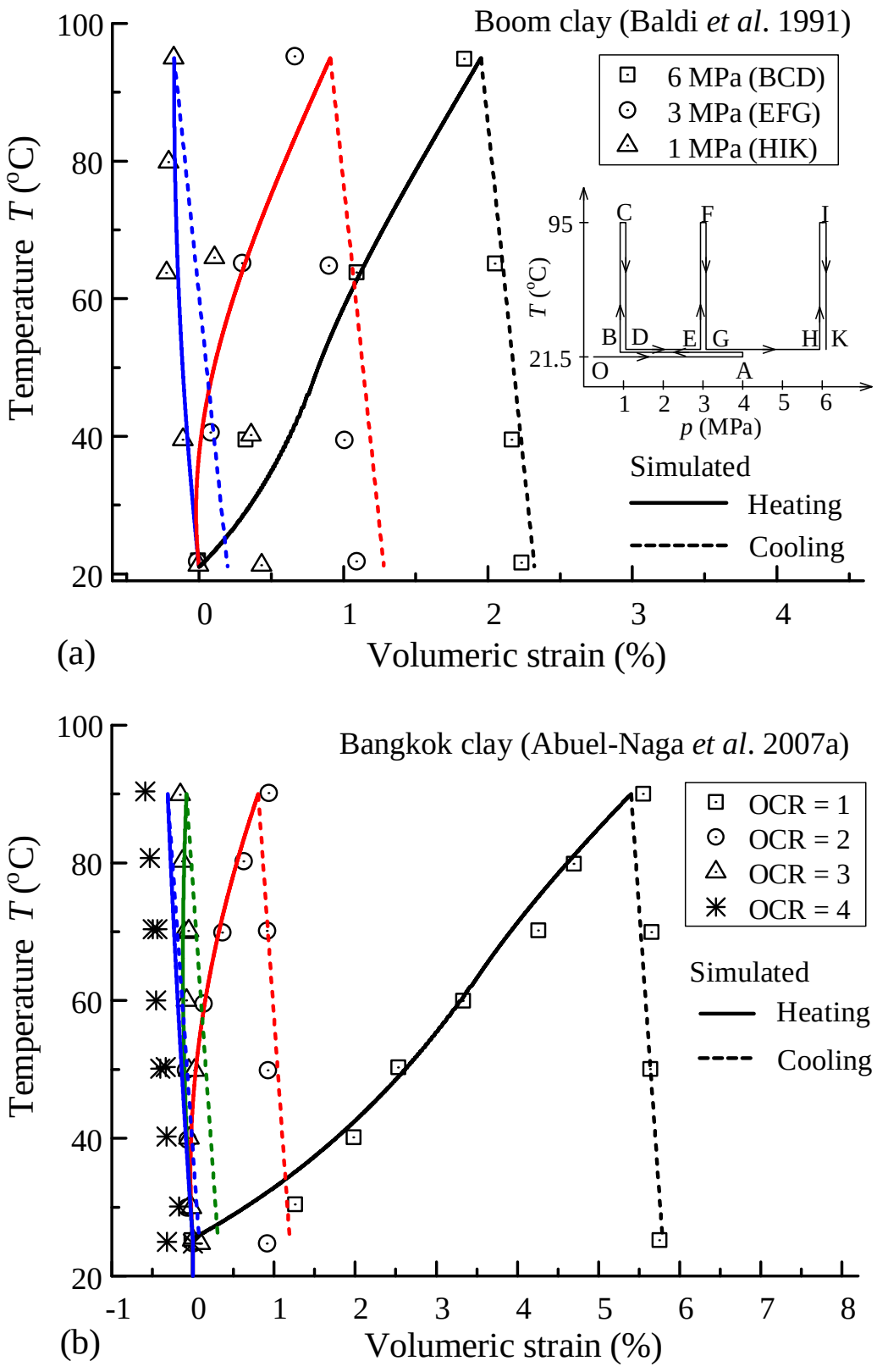

Fig. 9 Measured and simulated thermal volumetric deformation under heating-cooling cycle at different OCRs. (a) natural Boom clay (e_0 = 0.59); (b) Bangkok clay (e_0 = 1.4).

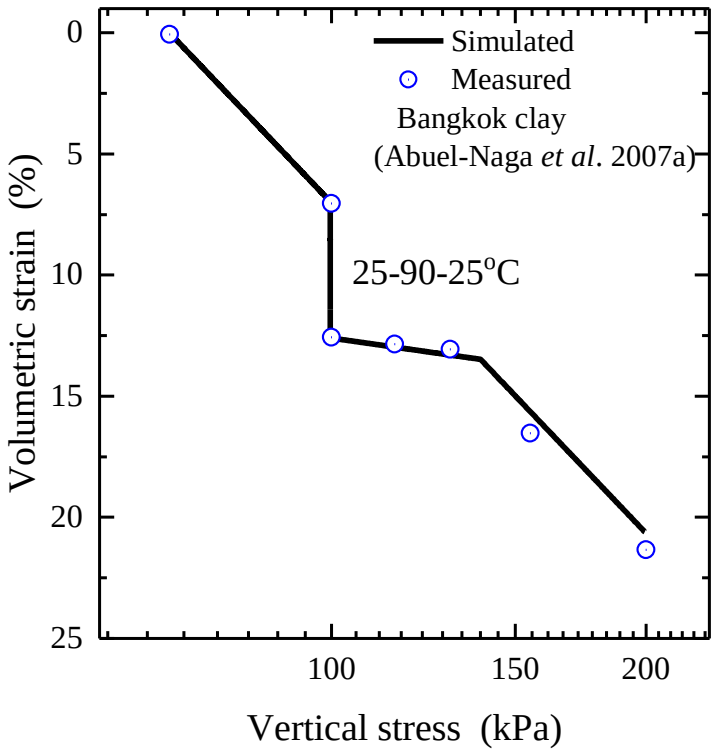

Fig. 10 Measured and simulated consolidation curves under a combined thermomechanical oedometric path.

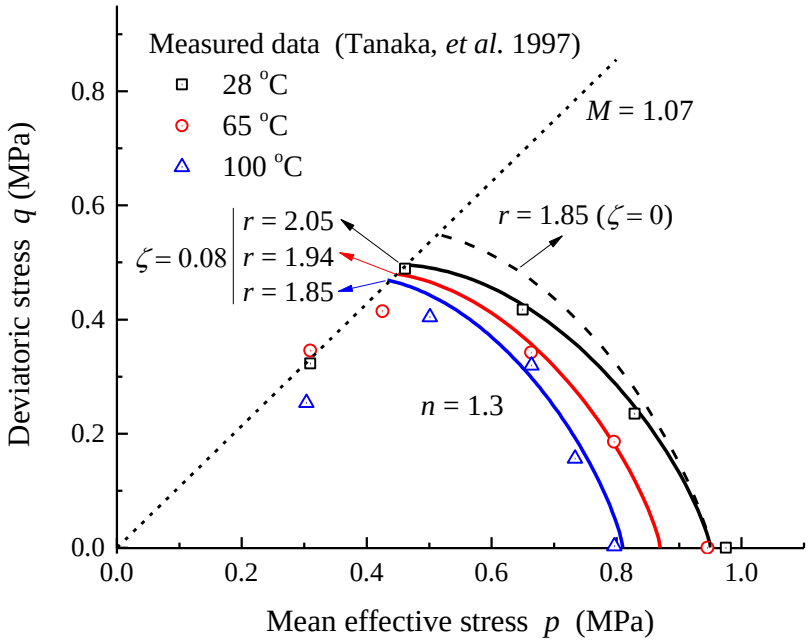

Fig. 11 Measured and predicted yield loci for Illite clay.

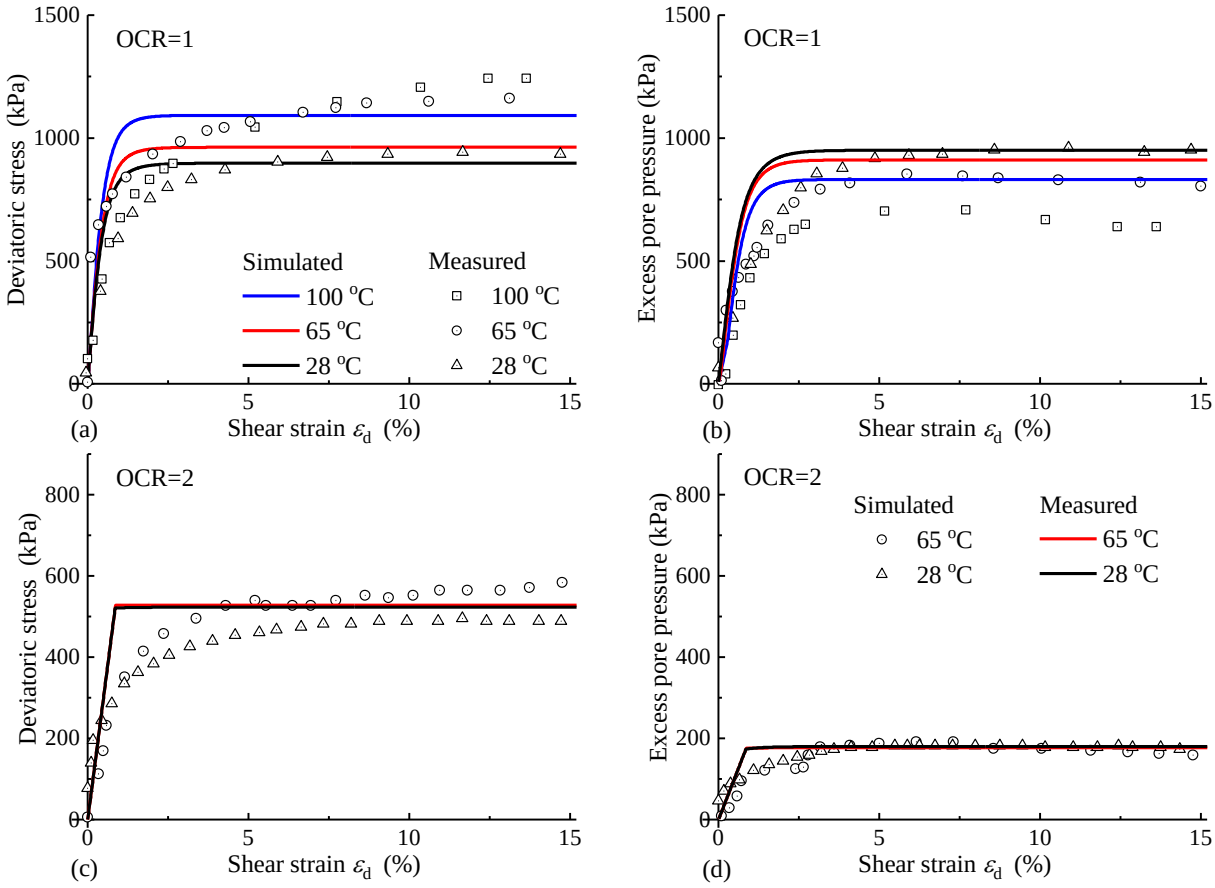

Fig. 12 Measured and simulated stress-strain curves for undrained triaxial tests on soft Illite clay at different temperatures (measured data from Tanaka (1995)).

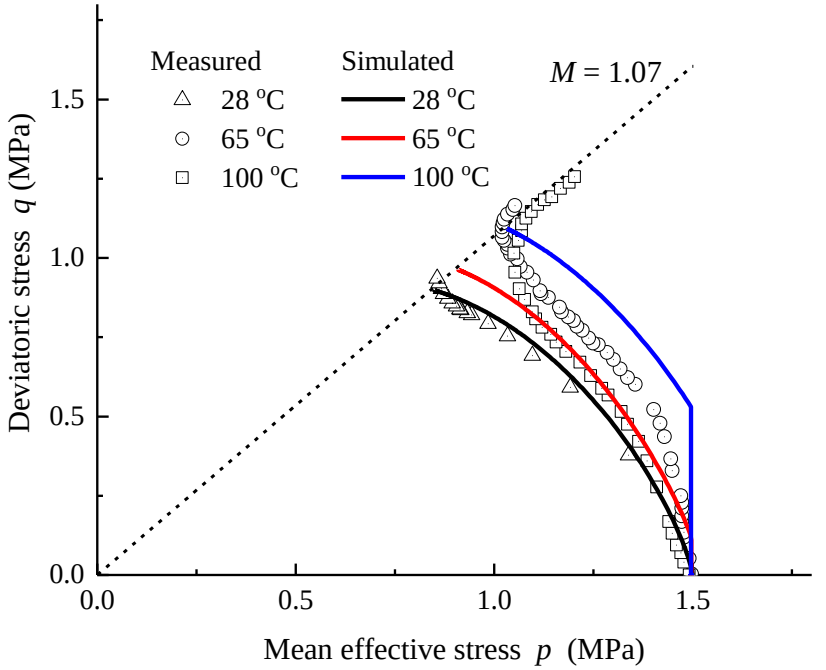

Fig. 13 Measured and predicted stress paths for normally consolidated Illite clay in undrained triaxial compression tests (measured data from Tanaka (1995)).

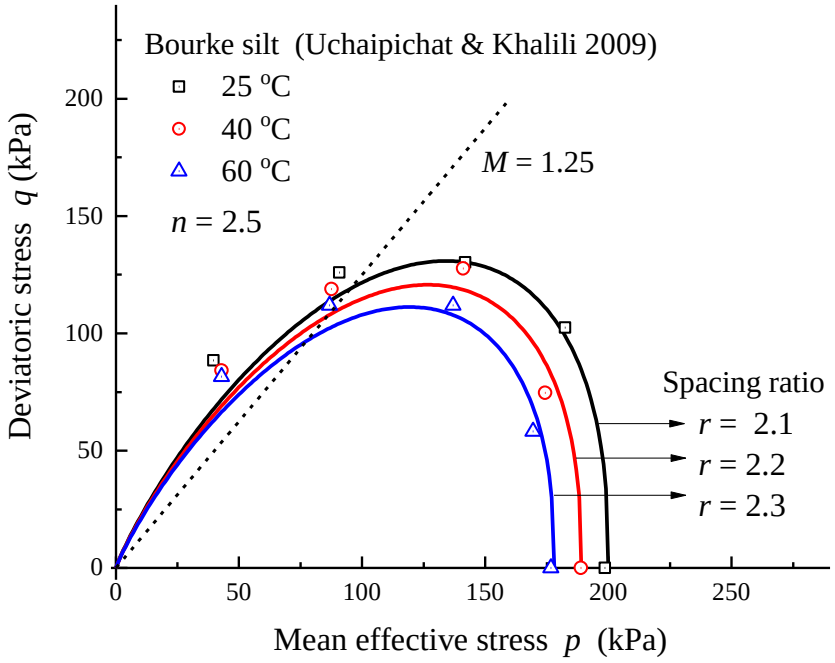

Fig. 14 Measured and predicted yield loci for Bourke silt.

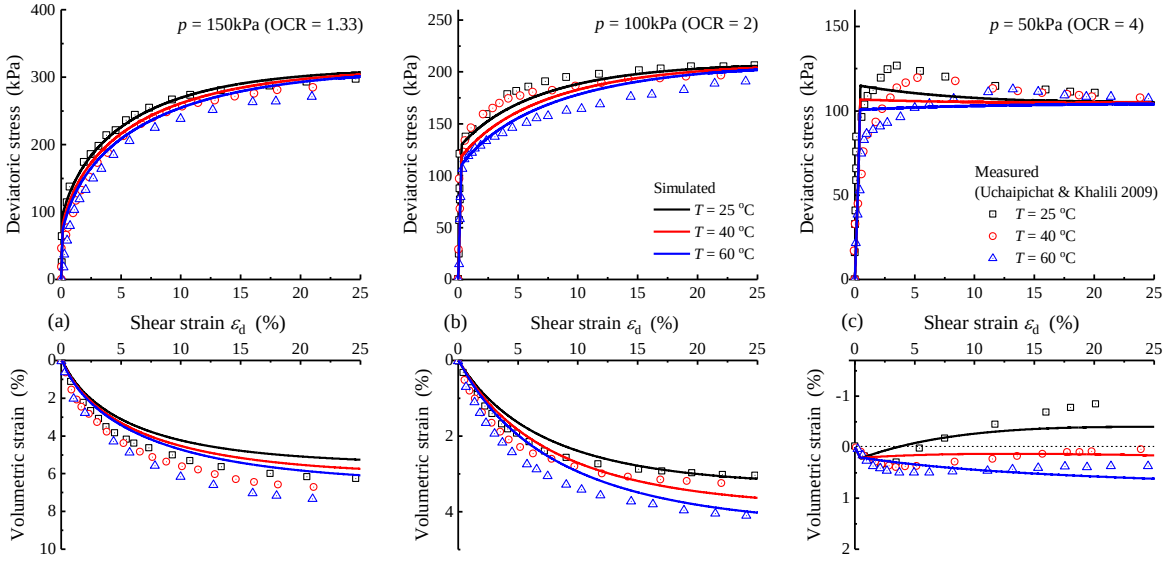

Fig. 15 Measured and predicted stress behaviour of Bourke silt in drained triaxial compression tests (e_0=0.56).